

ECMM102

Group Project (Meng) (A, TRM1+2 2017/8)

046138

1029797

**Coursework:** Individual contribution to the group achievement**Submission Deadline:** Mon 14th May 2018 12:00**Personal tutor:** Dr Julian Londono Monsalve**Marker name:** Tabor640025916 **Word count:** 13688

By submitting coursework you declare that you understand and consent to the University policies regarding plagiarism and mitigation (these can be seen online at www.exeter.ac.uk/plagiarism, and www.exeter.ac.uk/mitigation respectively), and that you have read your school's rules for submission of written coursework, for example rules on maximum and minimum number of words. Indicative/first marks are provisional only.

First marker's comments

Indicative mark

Second marker's comments

Second mark

Moderator's comments

Agreed mark



I2 Report

Investigation into Mesh Generation Techniques Using Pointwise® on Primary Sewage Sedimentation Devices.

Toby Alexander Scobell

2018
4th year MEng Group Project

I certify that all material in this thesis that is not my own work has been identified and that no material has been included for which a degree has previously been conferred on me.

A handwritten signature in black ink that reads "Toby Scobell".

Signed.....

College of Engineering, Mathematics, and Physical Sciences
University of Exeter

I2 Report

ECMM102

Investigation into Mesh Generation Techniques Using
Pointwise® on Primary Sewage Sedimentation Devices.

Word count: 13,688

Number of pages: 40

Date of submission: Sunday, 13 May 2018

Student Name: Toby Scobell

Programme: MEng Mechanical Engineering

Student number: 640025916

Candidate number: 046138

Supervisors: Prof Gavin Tabor

Dr Shenan Grossberg

Abstract

This individual report documents the meshing element of the group project ‘*Experimental and Numerical Investigation into the Use of Olive Stone Powder as a Substitute for Primary Sludge Modelling*’. [1] which uses the Armfield W7 Model Sedimentation Tank, and the Swirl-Flo® hydrodynamic vortex separator as case studies.

Computational Fluid Dynamics (CFD) code `driftFluxFoam` within OpenFOAM® uses finite volume method to solve multi-phase fluid dynamics problems using the Navier-Stokes equations. This numerical method requires a computational grid through which the equations are solved. Within this study, multiple meshing techniques are investigated using the commercial CFD grid pre-processing software Pointwise®. The aim was to create grids for both case study geometries, complying to strict mesh quality criteria pre-defined by `driftFluxFoam`’s solving algorithm. High fidelity structured, and hybrid Anisotropic Tetrahedral Extruded (T-Rex®) approaches were attempted for the Armfield Sedimentation Tank, and the Swirl-Flo® vortex separator respectively. All meshes were studied using both Pointwise®’s native ‘examine’ tool and OpenFOAM®’s domestic `checkMesh` function. The ability to automate and replicate grids were also driving objectives.

The structured mesh was proved to excel in all mesh quality checks. Mesh quality parameters such as non-orthogonality, volume ratio and skewness fell comfortably within quality criteria. An automation study was also completed, enabling small iterative changes to a completed topology. The unstructured mesh failed to meet the standards set by `driftFluxFoam`, because the non-orthogonal, anisotropic aspect of face elements within the boundary layer caused failed `checkMesh` results. Future development of T-Rex® or new techniques established in further study, may identify advanced automation capabilities robust enough to handle both iterative changes in topology and radical changes of design. These characteristics would be transformative when applied in industry. This modern, unstructured method would then prove superior to its dated structured counterpart.

Keywords: Primary Sedimentation, meshing techniques, Pointwise®, OpenFOAM®.

Acknowledgments

Many thanks to Professor Gavin Tabor for his support and guidance throughout the project. Thanks also to Dr Shenan Grossberg for his sustained assistance and direction, particularly when faced with the involved process of Pointwise®. I would also like to acknowledge input from Steven Daniels who provided an automated structured technique for the project.

Contents

1.	Introduction.....	1
1.1.	Aim.....	2
2.	Literature review	2
2.1.	Early Grids	2
2.2.	3D Structured Grids	3
2.3.	Unstructured Grids	4
2.3.1.	Unstructured Anisotropic Tetrahedral Extrusion.....	5
2.4.	Overset	6
2.5.	Hybrid.....	7
3.	Theoretical background	7
3.1.	Numerical Approach	8
3.2.	Courant Number.....	9
3.3.	Mesh Quality Parameters	9
3.3.1.	Skewness.....	9
3.3.2.	Non-Orthogonality.....	10
3.3.3.	Aspect Ratio.....	11
3.3.4.	Area Ratio	11
3.4.	Pointwise®	12
3.4.1.	T-Rex® Boundary Extrusion	12
3.4.2.	Automation with Glyph Scripting.....	15
3.4.3.	Elliptic Potential Difference Equation (PDE) Solver	15
3.5.	OpenFOAM.....	17
4.	Methodology and Results	17
4.1.	Architecture Study.....	17
4.1.1.	Methodology	17
4.1.2.	Results.....	18
4.2.	Geometry Creation	19
4.2.1.	Rectangular	19

4.2.2.	<i>Swirl-Flo®</i>	19
4.3.	Structured Mesh Creation – Settling Tank	20
4.3.1.	Convergence Study	20
4.3.2.	Scaffold	21
4.3.3.	Elliptic PDE Solver	23
4.3.4.	Boundary Layer	24
4.3.5.	Export	24
4.3.6.	Structured Grid – Rectangular Settling Tank	24
4.3.7.	Pointwise® Automation Study	25
4.4.	Hybrid Mesh Creation - <i>Swirl-Flo®</i> Tank	26
4.4.1.	Convergence Study	26
4.4.2.	Hybrid Scaffold	28
4.4.3.	T-Rex Block Initialisation	28
4.4.4.	Improved Hybrid Scaffold	32
4.4.5.	checkMesh Failure	33
5.	Discussion and conclusions	34
5.1.	Discussion	34
5.2.	Future Work	36
5.3.	Conclusion	37
6.	Project management	37
7.	Contribution to group functioning	39
8.	References	39

1. Introduction

Sewage is an omnipresent consequence of human existence; its treatment is a necessity for sanitation as growing populations and dense municipal communities increase pressure on infrastructure. A UK market research report published in January 2018 expects industry revenue to rise at a “compound rate of 1.3%” over the next 5 years to £8.4 billion, supporting 33,011 jobs within 941 businesses [2]. This economic influence attracts considerable research, mainly into improving the efficiency of treatment processes.

Sewage treatment uses a four-stage progressive approach: preliminary, primary, secondary and tertiary phases. This report considers only the primary stage of sewage treatment, the preliminary, secondary and tertiary treatment methods will not be discussed in detail. Following preliminary treatment in which floating debris is removed to protect the operation of the treatment plant [3], the primary or *sedimentation* stage focuses on separating solid-liquid flow. Sludge suspended in water is separated in large settling tanks or hydrodynamic vortex separators. Once separated, the products are treated by their constituent secondary and tertiary processes.

Whilst there are multiple ways to separate multi-phase flow, in sewage treatment reliance on the influence of gravity is paradigm. In settling tanks sewage is left to stagnate, and low volumetric flow rates allow settling of dispersed phase on the base of the tank. Tanks are normally equipped with mechanically driven scrapers, which continually guide sediment towards hoppers where it is pumped away for further treatment. Alternatively, a hydrodynamic vortex separator provides a compact, low energy cylindrical system. Operating hydraulically, solid-liquid flow is fed through a tangential inlet at high velocity, forming a vortex. The centrifugal inertia of solid matter in the flow is exploited. Contact with the cylindrical walls, causes it to decelerate and drop out of the vortex into an underflow, where sludge can be collected and taken away. Continuous phase passes through the top of the separator to an overflow tray and onward to the secondary treatment process. With no moving parts, and therefore a minimal maintenance requirement, operating costs are low.

Both systems have been subject to extensive empirical and, more recently, computational fluid dynamic (CFD) research. It is necessary for all computational models to be validated by an experimental investigation before computational analysis can begin. However, alternatives are required to avoid the unfavourable laboratory conditions associated with exposure to sludge

and other waste water derivatives. In 1992 Ellis et al [4] used Olive Stone Powder (OSP) as a sludge substitute. He noted that when OSP was used in a hydraulic scaled chamber, the location and depth of deposition concurred with that observed in an industrial chamber. Hydro International are interested in the use of OSP for conducting experiments. By empirically proving OSP as a suitable substitute, an accurate computational model could be created for design optimisation in further study.

CFD is a fast-emerging field that utilises both recent advances in computational power and a numerical approach to solving fluid problems. A computational geometry is developed using Computer Aided Design (CAD) to solve fluid equations through the application of various boundary and initial conditions. It is self-evident that solving continuum mechanics problems governed by potential difference equations through the application of computers, is paradoxical. This is the role of the mesh; a mesh is a discretisation of a continuous volume into a grid of cells. The Navier-Stokes equations are then integrated across the cell resulting in difference equations that can solved via forward, backward or central approximation.

1.1. Aim

The aim of this report is to investigate multiple meshing techniques in Pointwise®. Pointwise® is a mesh generation application created in 1984. It provides CFD pre-processing from geometry import to flow solver export. In this study structured, unstructured and hybrid meshing techniques are used to generate meshes for primary stage sedimentation tank and hydrodynamic vortex separator geometries. Quality and performance of each mesh is then analysed using Pointwise®'s internal examination techniques and OpenFOAM®. OpenFOAM® is an open-source CFD solver, providing codes for multiple flow types and post-processing functionalities. The results from various techniques are compared.

2. Literature review

2.1. Early Grids

The earliest examples of 2D structured meshes used the point-in-cell (PIC) Eulerian-Lagrangian technique. This used “fluid particles to transport mass, momentum and energy through an Eulerian mesh of cells.” [5] However, in their 1966 paper, Gentry et al presented one of the first Eulerian difference schemes across a discretised two-dimensional mesh [5]. This is more comparable with modern day techniques and used Fluid-In-Cell (FLIC) method

rendering particles unnecessary. This reduced memory storage requirements and computing time. The study attempted a replication of empirical work by Reichenbach et al [6] on the effect of reflected shock on a bomb shelter door through a z-shape tunnel using a scale model. The width of the experimental tunnel was 2 cm, and the lengths of the first and second legs were 8 and 8.8cm respectively. A two-dimensional, structured mesh was used for the design shown in figure (1a).

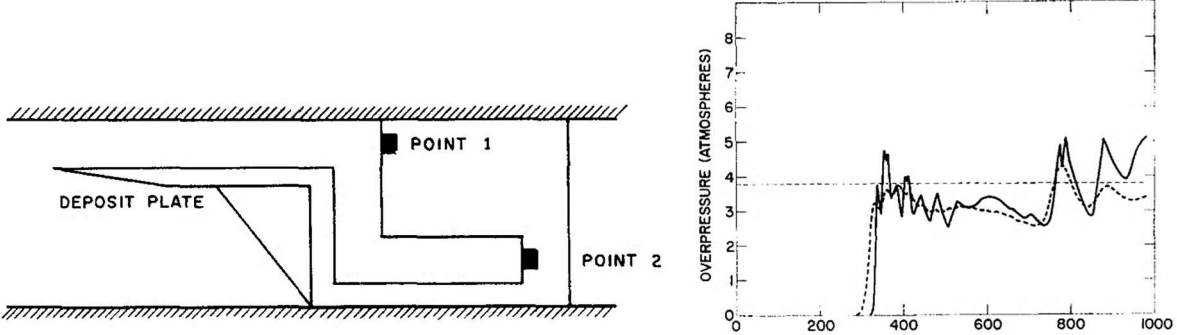


Figure 1 - a) Scale model of shelter access tunnel used by Reichenbach et al in their shock tube experiments. b) Comparison of experimental (bold) and numerically calculated (dashed) results.

The cells were square with an edge length of 2mm. Channel widths were therefore divided into 10 cells and a total of 1270 cells were in the domain. The FLIC transport model showed strong agreement, shown in figure (1b) in both curve shape and magnitude with Reichenbach et al's empirical studies for early time steps. Non-conformity between the two studies at later time-steps can be attributed to two-dimensional and shock-on-shock effects. Interestingly neither of these investigations used convergence studies to ensure accuracy of results, using experimental comparison as the only evidence of validity. This paper shows one of the earliest uses of CFD. Further developments in numerical modelling were conducted solely across 2-dimensional, structured meshes for the next 15 years.

2.2. 3D Structured Grids

The 3D structured mesh has been at the forefront of CFD development since the inclusion of structured hexahedral elements in PHEONICS, launched in 1981 [7]. A structured mesh relies on regular connectivity; therefore, the distribution of boundary points has been designed so the number of grid points on opposite boundaries are identical. In 3D this means 6 boundaries in the hexahedra offering both quality and control. “Structured” refers to the cell’s organisation within the array, such that a cells neighbours are implicitly known e.g. cell (I,J,K) has neighbours (I+1,J,K), (I-1,J,K) etc. This allows for neighbouring cells to be found directly via

the structure as opposed those in an unstructured mesh, where a connectivity table must be maintained and queried to find neighbouring points, resulting in an increase in computational performance [8].

In addition, R. Koomullil et al [9] found that structured meshes yielded more accurate results for viscous calculations because they can handle cells with a much higher aspect ratio in the viscous boundary layer. Structured meshes were also found to excel in both the memory and CPU requirements categories. This comprehensive study comparing both structured and unstructured meshing techniques provides key insights into the relative merits and demerits of both topologies.

In modern CFD, use of the structured grid is diminishing due to advances in the sophistication of the unstructured mesh, and large increases in computational capacity which handle its less efficient composition. An inflexible, difficult to adapt topology is seeing its prominence challenged, in an industry impatient for results. In competitive markets, the desire for rapid generation supporting iterative prototype improvements, has directed commerce away from the structured grid. However, John Chawner, Pointwise, Inc., a front-line expert in cutting edge meshing progression, sees a place for structured grids in the future of CFD. He states that “structured grids aren’t going away” [9], because of their merits of resolution, alignment, definable norms, and time and memory reductions.

2.3. *Unstructured Grids*

The unstructured mesh offered a new, appealing and flexible approach to grid generation. Its ability to quickly conform to any geometry, simple or sophisticated, was instantly appealing to the industry. Comprised of mainly tetrahedral cells, it can effectively implement any cell with any number of edges and faces. Since 1995 when D. J. Marviliis called unstructured mesh generation a “solved field” [10], vast progression in the automation discipline has seen codes such as CFMesh® and SnappyHexMesh® further the work of pioneers such as Delaunay. The introduction of a bounding box when working with Reynolds-Averaged Navier-Stokes (RANS) generated grid has been found to reduce the CPU times in mesh generation by 24 times. The bounding box reduces the complexity of storing data on 3D background grids to that of a 2D problem. Only six faces of a bounding box are used as a storage device, allowing faster referencing times and lower storage requirements [10].

Past work on cyclone separators using an unstructured mesh has shown promising results. Turbulence modelling by Slack et al [11] showed they could accurately replicate turbulence

using both RSM and LES turbulence models on a vortex separator geometry. Run on a 40,000 and 640,000 cell unstructured meshes respectively, they found that the finer mesh revealed time dependant vortex oscillations which potentially impact the separation efficiency and wall boundary layer.

Issues associated with basic unstructured techniques have been addressed in modern research. The introduction of innovative Anisotropic Tetrahedral Extrusion (T-Rex[®]) method addresses boundary layer resolution and aspect ratio issues. Increases in computational capability have offset increased costs of running simulations on unstructured meshes.

2.3.1. *Unstructured Anisotropic Tetrahedral Extrusion*

T-Rex[®] was designed to grow high quality anisotropic cells from watertight quadrilateral and triangular surface meshes. The boundary layer, usually composed of tetrahedral prisms and hexahedra, is grown until isotropy is reached. The rest of the volume is then initialised with isotropic unstructured tetrahedral cells using a modified Delaunay volume mesher. A webinar performed by Travis Carrigan and Mark Landan, Pointwise, Inc., [12] showcases the efficacy of T-Rex through the application of the DrivAer case. Initially developed by the Institute of Aerodynamics and Fluid Mechanics at the Technische Universität München, the DrivAer model sets the industry benchmark for current meshing capabilities. Within the webinar, the DrivAer geometry is meshed using Pointwise and the results described as ‘high quality’, setting the benchmark for Pointwise[®] (figure 2). It should be noted that OpenFOAM[®] and T-Rex[®], due to disparity in age, often appear incompatible. For example, when the mesh generated within the webinar is run through `checkMesh`, 703 non-orthogonal faces are highlighted [13]. The webinar addresses this challenge, noting that centroid skewness parameter within Pointwise[®] should be below 0.7 when applying T-Rex[®] for OpenFOAM[®].

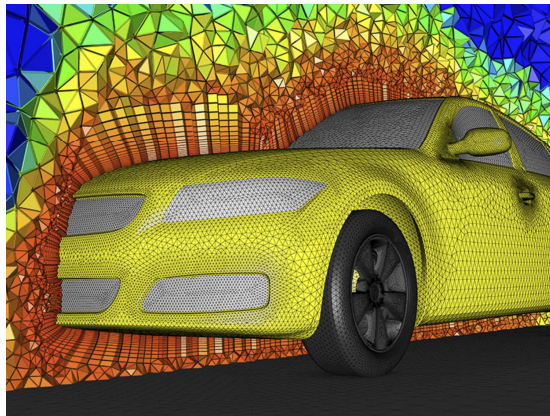


Figure 2 - The T-Rex extruded DriveAr mesh used in the Pointwise webinar.

Although in the early stages of development, T-Rex® has been used with unstructured meshes, to replace structured meshes in multiple papers. In another OpenFOAM® case, Prof. Rickard E. Bensow [14] used T-Rex® for a “smooth transition to tetrahedra” between a complex hull geometry into a fluid domain. The mesh totalling 19,626,440 cells was run across 64 cores and its results were found to “capture and agree qualitatively” with published results on open water propeller/rudder interaction. Bensow’s study used T-Rex® with OpenFOAM, and therefore had equivalence with this investigation. However, the significant computational power at Bensow’s disposal allowed for higher fidelity, OpenFOAM® compatible T-Rex® grids.

2.4. *Overset*

Overset meshes are an historical structured approach to complex geometries. The computational domain can be modelled by overlapping component meshes. The flexibility of multiple overlapping structured grids, simplifies the construction of complex geometries. The overset meshing technique is widely used in simulations with moving bodies, but can improve overall cell quality in some static situations.

Faranggis Bagheri, Pointwise, Inc., [15] conducted a comparison study on meshing techniques between overset and T-Rex® (see section 2.3). Creating an expression for efficiency

$$\eta_{sim} = (1 - \varepsilon)^3 \left(1 - \frac{t_{manual}}{t_{ref}}\right) \quad (1)$$

Where ε is error in the solution, t_{manual} is time to manually create the mesh, and t_{ref} is the time to complete one full overset mesh strategy (create, set up the simulation and run it). The Schiffbau-Versuchansalt (SVA) model VP1304 propeller, aka the Potsdam propeller Test Case was used as a model. The T-Rex® model was found to have an error of 1.63% on average and the overset technique average of 3.03%, when compared to experimental results for torque and thrust. The total times taken to set up the mesh, the case file and to run the simulations were 33h 3mins (28h 30mins set up and 4h 33min run time), and 2h 34mins (1 hour 1min setup and 2hr 34min run time) for the overset and T-Rex® cases respectively. Putting these values into the expression for efficiency, the T-Rex® case was found to be 93.3% efficient compared to the overset case value of 12.5%. Note that the overset case is not described as 0% efficient as the simulation run time enables the engineer to step away from the computer to complete other tasks. This study found the T-Rex® case to be more efficient than the overset meshing technique, however, this would not be true for all cases. When using the overset technique,

quality is guaranteed due to unrestricted topologies. Therefore, for a highly complex case the overset technique may be a better method.

2.5. Hybrid

When applying a hybrid mesh, the geometry of the volume is considered and the most suitable type of mesh is applied to each block. This, in theory, allows the engineer to apply whichever meshing technique has the best combination of attributes for each individual circumstance. The regular and irregular portions of the grid will be structured and unstructured respectively. Most modern-day research uses a hybrid approach to create the most efficient, high quality mesh.

“Hybrid Grid Generation for Turbomachinery” [16] demonstrates how a hybrid grid for a combined inlet torus and nozzle ring for a steam turbine can be completed in the order of hours. The mesh consisted of approximately 350,000 prisms, 3,000 pyramids and 1,680,000 tetrahedra. This hybrid mesh showed good agreement with experimental data. Figure 3 compares computed static pressure distribution (p_0) with Streamwise Position (m), for both numerically derived and experimental data.

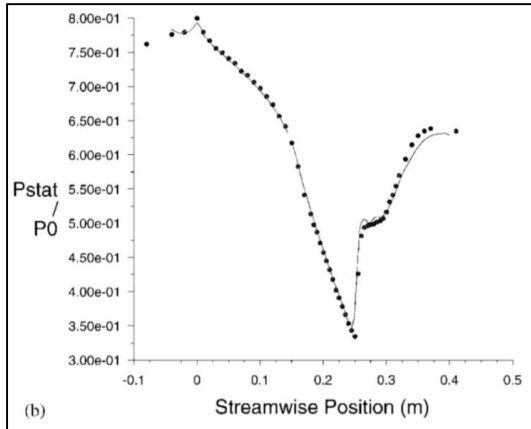


Figure 3 - Computed static pressure distribution (p_0) against streamwise position (m)

An unstructured grid cell count is generally far higher than a hybrid one. Pointwise, Inc. found that hybrid grids generally use 43% of the total cells when compared to an unstructured grid of cells with a similar volume [17]. By applying a structured grid to regular segments of the geometry, dramatic cell reductions are possible.

3. Theoretical background

3.1. Numerical Approach

CFD logistics are governed by the Navier-Stokes equations, these equations solve fluid flow problems through the implementation of Newton's second law. In full, the equation can be represented as

$$\rho \left(\frac{\partial \mathbf{u}}{\partial t} + \mathbf{u} \cdot \nabla \mathbf{u} \right) = -\nabla p + \nabla \cdot \left(\mu (\nabla \mathbf{u} + (\nabla \mathbf{u})^T) - \frac{2}{3} \mu (\nabla \cdot \mathbf{u}) \mathbf{I} \right) + \mathbf{F} \quad (2)$$

Where \mathbf{u} is velocity, p is the field pressure, ρ is the fluid density, μ is the fluid dynamic viscosity and \mathbf{F} is external forces. Each term in the equation corresponds to the forces experienced in fluid flow; inertial forces, pressure forces, viscous forces and external forces respectively. Because of this, it can be easily simplified through the application of assumptions such as incompressibility or adiabatic flow. These equations are always solved together using the continuity equation.

$$\frac{\partial p}{\partial t} + \nabla \cdot (\rho \mathbf{u}) = 0 \quad (3)$$

By solving both equations simultaneously, momentum and mass are conserved.

In a time-dependant case such a parabolic, transient problem, time must also be discretised. This is done by time marching. The time derivative is discretised using the forward Euler method. The approximation can be found via the application of the Taylor series.

Let t_s , $s = 0, 1, 2, 3, \dots$, be a sequence in time with

$$t_{s+1} = t_s + \Delta t \quad (4)$$

Let y_s and Y_s be the exact and approximate solution at $t = t_s$. To obtain Y_{s+1} from (t_s, Y_s) the differential equation must be used. Since the slope of the solution to the equation $y_t = f(t, y)$ at the point (t_s, y_s) is $f(t_s, y_s)$, the Euler method determines the point (t_{s+1}, Y_{s+1}) by assuming it lies on the line through (t_s, Y_s) with the slope $f(t_s, Y_s)$. Therefore, the formula for the slope of the line is

$$t_{s+1} = t_s + \Delta t \frac{\partial s}{\partial t} \quad (5)$$

The solver will then invert the resulting large matrix into a solution, and repeat the process for as many timesteps as necessary until convergence is reached [18] [13].

Equations (2) (3) (4) and (5) all require a discretised grid to produce a solution. The concept of meshing is an often overlooked but vital aspect of the CFD process. The mesh provides the

platform that enables the solver. Whilst it doesn't directly produce results, the quality of the mesh directly affects the accuracy of the harnessed data.

3.2. Courant Number

The Courant-Friedrichs-Lowy condition is a measure of stability when solving PDE's numerically by the method of finite differences. Its principle dictates that if flow is moving through a discretised, spatial grid where characteristics of the flow are to be measured at discrete time-steps of equal duration, then this time must be less than the duration for the flow to travel between adjacent grid points [19]. Usually illustrated by the courant number, for stability it must total less than or equal to one. It can be calculated by the equation

$$C_r = \frac{\mu \Delta t}{\Delta x} \leq 1 \quad (6)$$

Where μ is the magnitude of the velocity, Δt is the time step and Δx is cell size in the direction of velocity.

3.3. Mesh Quality Parameters

As mentioned in section 3.1.1, the mesh influences the accuracy of the solution. However, each solver is different and has different requirements regarding grid topology. Because there is no rigid law for definitions and max/min values for these parameters, each metric must be defined using general rules to gauge relative mesh quality.

3.3.1. Skewness

3.3.1.1. Equiangle Skewness

Equiangle skewness is represented as the “maximum ratio of the cell’s included angle to the angle of an equilateral element” [20] in degrees. It has minimum/maximun value of 0 and 1 respectively. It is good practise to keep this below 0.8 for a good grid; values below 0.9 are acceptable, depending on the solver. Equiangle skewness is equivalent to FLUENT®'s own skewness criteria.

It can be computed as follows:

$$\max \left[\frac{(Q_{\max} - Q_e)}{(180 - Q_e)}, \frac{(Q_e - Q_{\min})}{Q_e} \right] \quad (7)$$

Where Q_{max} is the largest angle in the cell, Q_{min} is the smallest angle in the cell and Q_e angle for an equilateral element (60 for Triangle, 90 quadrilateral). This skewness criteria applies to 2D surface meshes to check quality and is less informative for block cells.

3.3.1.2. *Centroid Skewness*

Centroid Skewness is defined as “1 minus the maximum dot product between the cell face normal and the vector connecting the cell centroid and the face centroid” [20]. It measures the extent to which a cell is collapsed and is a useful metric for measuring the success of the T-Rex® boundary extrusion. Values range from 0 (no-skew) to 1 (collapsed cell).

This measure of skewness is particularly important when solving using OpenFOAM®. OpenFOAM® calculates fluxes between cells from face normal vectors for finite volume schemes. Therefore, multiple correcting loops would be required to solve a mesh with a centroid skewness value larger than 0.7. This would slow convergence rates and may even cause diversion. As well as computational savings, Zang et al [21] mention that a large proportion of highly skewed cells could result in a deterioration in accuracy comparative to a reduction from a second to a first order differencing scheme.

3.3.2. *Non-Orthogonality*

Orthogonality is defined as the deviation angle between the vector from the cell centroid to the centroid of each of the adjacent cells, and its corresponding face normal [22]. It therefore has a scale from 0° (a perfectly orthogonal mesh) to 180° (a highly distorted cell). An OpenFOAM® metric, it is incalculable within Pointwise® as it uses face information. Pointwise® does not store faces, only points and cells. OpenFOAM® considers any cell with a non-orthogonality metric of 70° or higher as non-orthogonal [22]. Where there are cells with a value above 70°, convergence of a solution is likely to be inhibited.

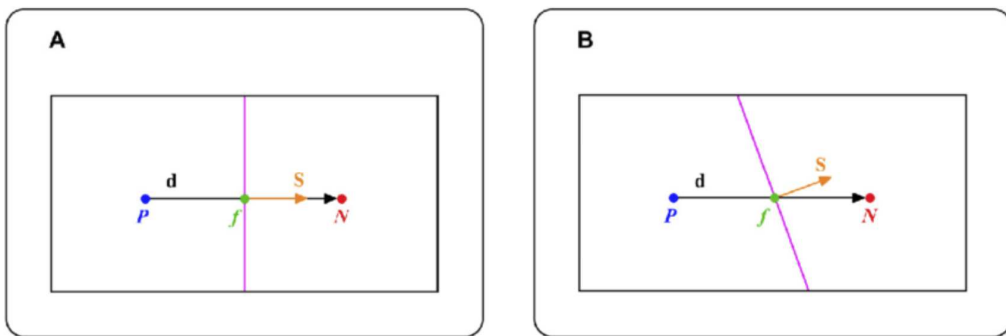


Figure 4 - a) An orthogonal connection between cells. b) A non-orthogonal connection between cells.

Within OpenFOAM®’s approximation numerics, the vector connecting the cell centroids (shown in figure 4 in black) represents the approximation of the gradient across the shared face. When non-orthogonal cells are adjacent, the vectors can become mis-aligned causing significant errors in the dot product of the gradient with face area.

3.3.2.1. Maximum/Minimum Included Angle

The maximum/minimum included angle is a skewness metric. Pointwise® recommends its use to indicate whether a cell is non-orthogonal. It is fair to assume that a cell with extreme maximum/minimum interior angles will have a high non-orthogonality. Therefore, it is common practise to assume both metrics have a similar effect on the numerics of the solution. The ideal value of $\theta = 90^\circ$ with a variance of $45^\circ < \theta < 160^\circ$ for a quadrilateral element and an ideal value of $\theta = 60^\circ$ with $20^\circ < \theta < 150^\circ$ of variance for a triangular element is acceptable [23].

3.3.3. Aspect Ratio

The aspect ratio of a cell is the ratio of the longest to the shortest side in a cell. An ideal value equalling 1, it governs solver ability to effectively interpolate between the centroids of a cell and its faces. Large aspect ratio can result in an interpolation error of unacceptable magnitude in areas of multidimensional flow. However, it has been found that large aspect ratio in regions of anisotropic flow have yielded more accurate results and faster than a constant ratio of 1, due to courant and timestep savings [24]. In areas where a large aspect ratio is unavoidable, for instance within the viscous boundary layer, quad/hex elements are favoured over the triangle/tet alternative, due to their ability to maintain a low level of skew [9]. In general, keeping maximum aspect ratio below 100 is acceptable [23].

3.3.4. Area Ratio

The area ratio of a mesh is a 2D ratio of adjacent cell areas. Known commonly as smoothness, it describes the transition between adjacent cell areas, as the solver works through the grid. Just like aspect ratio, the “ideal value” for area ratio may change depending on the specifics of the flow. When within the viscous boundary layer, an area ratio of no higher than 2 is expected [25], however in bulk flow it should not exceed 1.2 [26]. Whilst extreme values are not recommended, the area ratio can be determined by the analyst’s best judgement. The decisions should be influenced by a sensitivity study on the relevant flow field.

3.4. Pointwise®

Pointwise, Inc. creates commercial mesh generation software for pre-processing in CFD. Pointwise® applies GRIDGEN®, a U.S Air Force sponsored grid generation software est. 1984. Commercialised in 1994, its time-tested suite of meshing products is applied with a modern, intuitive GUI [27]. An arsenal of meshing techniques can be generated including structured hexahedral, unstructured tetrahedral, hybrid and overset meshes discussed in section 2. Its compatibility with nearly all CAD and CFD solver interfaces making it almost universally useful to CFD engineers. It adopts a *bottom-up* meshing approach, reciprocal to *top-down* or automated unstructured grid generation techniques, implemented by competitors such as SnappyHexMesh® and CfMesh®. The approach dictates that grid distributions are defined, 2D domains are created and then grouped into 3D blocks and initialised. This allows enhanced control of mesh quality but requires increased investment in user skill development. Widely recognised as one of the best meshing packages for structured grids, Pointwise®'s development of T-Rex® for boundary layer resolution in unstructured meshing was released in v17 in 2012. Firmly established at the top of both structured and unstructured markets, its versatility with both forms of mesh, enhances its ability to create strong hybrid grid topologies.

3.4.1. T-Rex® Boundary Extrusion

3.4.1.1. Theory

As discussed in section 2.3.1, T-Rex® was designed to grow high quality anisotropic cells from watertight unstructured quadrilateral and triangular surface meshes. It works by marching nodes off a surface by a user defined wall spacing, creating an anisotropic right-angled tetrahedron shown in figure 5. Before the vertex is saved, the tetrahedron is evaluated for negative volume, collision with other encroaching marching fronts and user defined mesh quality constraints. Should any of these be violated, the vertex is disqualified, and position adjusted via Steepest Descent Method to find a new location. If the new vertex location still fails, the front is stopped locally. The exception is in the case of isotropy, this prevents anisotropic cells in the normal direction to the surface. This process is repeated, forming layers of stacked right-angle tetrahedra until all vertex advancements are stopped or reach isotropy. Off the isotropic front, the block is populated with tetrahedral cells via a modified Delaunay method.

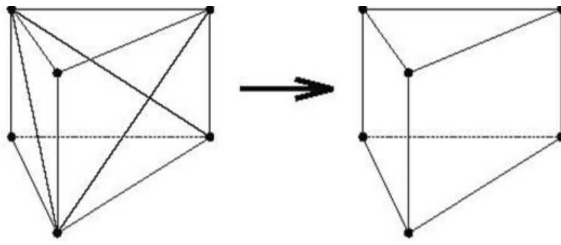


Figure 5- The combination of anisotropic tetrahedra into triangular prisms.

With the launch of v18, two adjacent tetrahedral elements can be combined further into a triangular prism, reducing the local cell count by a factor of 6. Cell count can be reduced by up to 67% [28] through the introduction of T-Rex® using this method.

3.4.1.2. Layer Functions

Maximum Layers – ‘Max Layers’ defines the total anisotropic tetrahedra layers. It is recommended that this value is set larger than the user expects to need for a case. This guarantees all cells are grown to isotropy for a smooth blend to the unstructured tetrahedral block. Applies to domains set to a T-Rex® ‘wall’ boundary condition.

Full Layers – Denotes the number of layers forced off the triangulated surface. It is useful to ensure an even layer of prisms/hexes in the boundary layer. It is usually set to a value an order of magnitude lower than maximum layers, and applies to domains set to a T-Rex® ‘wall’ boundary condition.

Growth Rate – Specifies the rate at which the layers march from the triangulated surface. It’s important within a hybrid mesh that this growth rate matches that of structured interior domains set to a T-Rex® ‘match’ boundary condition.

Push Attributes – Automatically propagates the block T-Rex® attributes to unstructured domains set to a T-Rex® ‘match’ boundary condition. The initial spacing, number of layers and distribution of points on the interior of the T-Rex® block will automatically be matched. This function offers some of the advantages of *top-down* meshers such as SnappyHexMesh®.

3.4.1.3. Advanced Parameters

Isotropic Seed Layers – When the marching front is stopped by skew criteria, isotropy is not reached, meaning highly skewed cells may be present at the prism/tetrahedral interface. This function determines how many “seed layers” or vertices are marched through the tetrahedra from the layer front with the aim of dividing large, highly skewed cells into smaller more orthogonal ones, smoothing the transition. The vertices are marched based on growth rate and layer height. Its default setting is off, or 0.

Collision Buffer – Invaluable in meshing complex geometries, the collision buffer specifies a buffer, or a gap to be maintained between encroaching fronts. The user specified number defines the buffer by multiplicative factor of the current cell height. Using this function leaves room for regular, uncompressed tetrahedra in the volume, relieving stress on skew criterion.

Aniso-Iso Blends – Controls the rate at which cells are decimated as T-Rex® layers are marched off a surface mesh (vertices removed as a front progress, reducing cell count), ensuring a blend from anisotropic surface meshes to isotropy. Usually left at its default setting of 0.5, its use is only helpful when large numbers of anisotropic cells are present on the surface mesh.

3.4.1.4. Skew Criteria

Skew criteria attributes are used to enforce additional quality control measures on newly formed anisotropic tetrahedra. Should the new anisotropic cell violate these criteria, they are modified to attempt to satisfy the constraints. If no viable solution is found, the element is discarded, and extrusion terminated locally. It is possible to set skew criteria for Maximum Included Angle, Equi-Volume Skewness, Equi-Angle Skewness and Centroid Skewness. Reference section 3.1.3 for more information.

Delay Skew Criteria – This function delays quality checks being made before a pre-set number of layers are completed. The value must be less or equal to the defined number of maximum layers.

Smoothing

These options control how smoothly the T-Rex® transitions between areas of different initial step size and is controlled by 2 functions. The region, or area of influence, in which the T-Rex® layers transition is controlled by the Relax factor, whereas the smooth parameter defines the number of Laplacian iterations applied to the growing T-Rex® region.

Boundary Condition

The boundary conditions tab allows the user to define where T-Rex® layers should be grown and specify the initial layer height (Δs). There are three types of boundary condition available for the T-Rex® algorithm.

Wall – Sets a domain to have anisotropic tetrahedra grown from that boundary. A Δs value should be specified.

Match – Sets domains on which the distribution of points should match the interior anisotropic tetrahedra. The match boundary condition should be applied to domains binding those with a wall boundary condition.

Adjacent Grid – Sets a domain to have anisotropic tetrahedra grown from it, while matching cell height to an adjacent block. This function is useful when applying T-Rex® to hybrid grids, allowing a smooth transition from structured hexahedra to unstructured hexahedra.

3.4.2. Automation with Glyph Scripting.

Pointwise®’s Tcl-based scripting language, Glyph, brings automation to the software package. Covering the entire range of commands available on Pointwise®’s GUI, it can be used to streamline processes such as the creation of a structured OH topology [29] (macros), or create full topologies such the creation of hexahedral, multi-block grids as shown by M.W. Tufts et al’s [30] stability based turbulent transition predictions on HiFire-5 aerofoils (templates). Discussed further in section 4.3.7, this feature, coupled with Pointwise®’s capabilities, makes it an extremely powerful optimisation tool.

3.4.3. Elliptic Potential Difference Equation (PDE) Solver

When working with structured grids, the elliptic solver can be used to smooth cells and increase mesh quality. The solver calculates the solution to Poisson’s elliptic partial differential equations (PDE). Multiple parameters are available to the user for complete control of grid points and mesh distribution.

3.4.3.1. Solution Algorithm

The solution algorithm is iteratively applied to a grid to locate node positions. They are found using a successive over-relaxation (SOR) usually in parallel with multi-grid acceleration. Several iterations can be specified by the user to improve grid quality. SOR is an explicit variant of the Gauss-Seidel model, and is used to solve any linear system of equations computationally.

Multi-Grid - The application of multi-grid can dramatically improve convergence times. It applies a global correction to coarser and coarser representations of the original grid until the cost of a direct solution is negligible compared to the cost of one relaxation sweep on the fine grid. Each correction is propagated through to the original mesh in real time [31].

3.4.3.2. Interior Functions

Interior control functions are used to influence the distribution of grid points on the interior of the grid. Within Pointwise®, three functions are available:

Laplace – Provides a very smooth distribution of grid points, however, no degree of orthogonality of the clustering is provided [32]. This is because each point’s position is based on that of its neighbours, enforcing smoothness to the detriment of orthogonality.

Thomas-Middlecoff – Grid points are clustered on the grids interior based on how the grid points are clustered at the boundaries, therefore orthogonality is enforced. This reliable, stable method is the default setting in Pointwise® [33].

Fixed Grid – Grid line slope discontinuities are eliminated whilst preserving the rest of the grid. Very subtle in its effects, this method should not be used unless the starting grid is of adequate quality except for discontinuities.

3.4.3.3. Boundary Functions

Boundary control functions influence the distribution of grid points so grid points one layer inward from boundaries will satisfy a specified spacing and angle constraint. Because there are multiple options for defining these constraints, they are not discussed in this report. For the majority of structured grid smoothing in this project, spacing and angle boundary information was taken from an adjacent grid. All other interior points are blended smoothly, three options are available:

Von Lavante-Hilgenstock-White – This method yields almost exact enforcement of the specified constraints; however, the grid may lack the smoothness provided by the Steger-Sorenson model [34] [35] [36].

Steger-Sorenson – A smooth, clustered and orthogonal boundary is produced by this function at the detriment of constraint accuracy. This was used throughout the project [37].

None – No conditions are applied to the boundary, allowing all points to be formulated from the interior function algorithm.

3.4.3.4. Edge Functions

The elliptic solver does not move points on connectors by default. However, in a common instance of the solvers application, moving points on connectors is advantageous. Three options are available:

Fixed – Edge points are unaffected by the elliptic PDE solution.

Floating – Both points on connectors *and* edge shape of connectors will “float” as if they are interior grid points to conform to the PDE’s optimal solution. This function is only applicable if a unique neighbour to the edge is found. Should no neighbour be found, the condition is converted to fixed [38].

Orthogonal – Points on connectors will move to maintain orthogonality with interior grid points. Edge shape remains fixed [38].

3.5. *OpenFOAM*

OpenFOAM® is an open source, numerical CFD solver, used by both industrial and academic organisations. Written in C++, it's a cell centred code that uses normal at face centroids to progress between cells. Known for being highly sensitive to flow conditions and mesh quality, the code scores poorly on robustness against commercial rivals such as FLUENT and ICEM. It has a range of solvers for various flow types and has both pre-process and post-process capacities. It is the solver of choice for this project.

4. Methodology and Results

4.1. *Architecture Study*

Since computational efficiency would have a key influence on the project, a study of the Exeter University CEMPS 28 core blade server architecture was conducted. This provided a better understanding of achievable core interaction times. All simulations within the G2 [1] aspect of this report were conducted over multiple cores, spreading the work load. However, should a mesh be split across too many cores, increased interaction times will result in diminishing returns. This is known as Amdahl's law and is discussed in the ACM Computing Survey journal [39].

4.1.1. *Methodology*

A cylindrical grid with a structured OH topology was created for simulating basic pipe flow. The mesh consisted of 288,000 cells, chosen as it offered a good range of values either side of the 40,000 cells per core rule of thumb suggested by the project client. A `simpleFoam` case was set up and was repeatedly run across 1-28 cores. Execution time (computing time) and clock time (total time for the simulation to run) were the dependant variables in this study. Interaction time (total time for communication between cores) could then be derived from the difference. The range for elements per core is 288000 – 10286.

4.1.2. Results

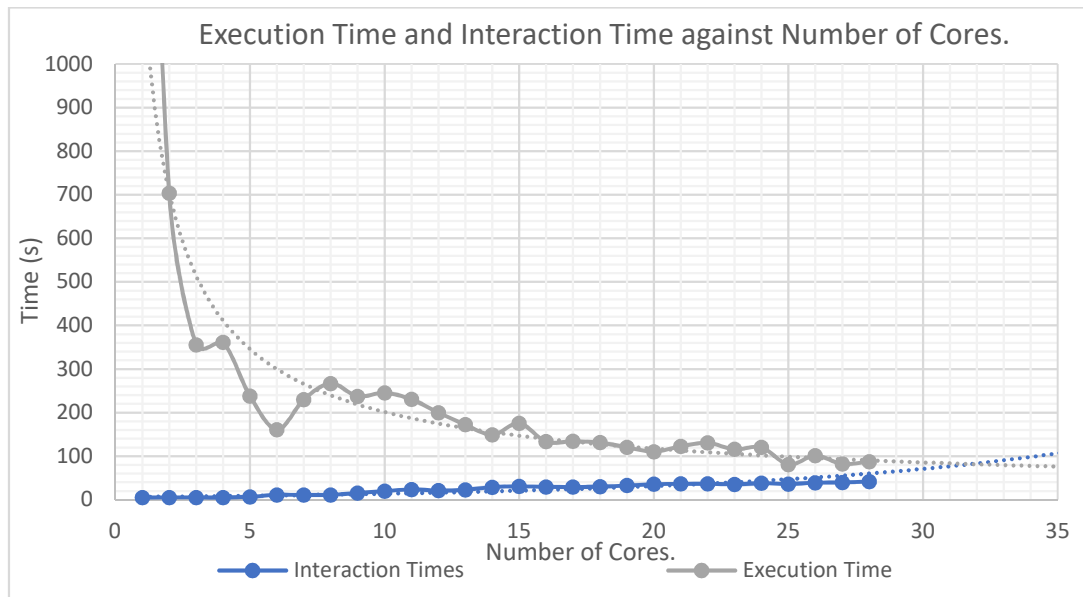


Figure 6- Clock and Interaction Time against Number of Cores.

Figure 6 shows an initial dramatic reduction in execution time as the number of cores grow. The gradient flattens however, as the number of cores increases further. The interaction time increases exponentially as the number of cores grows. Forecasts were placed to predict the point of intersection. It can be seen that at ≈ 32 cores, the interaction time will grow larger than the execution, therefore predicting negative returns at around 9000 cells.

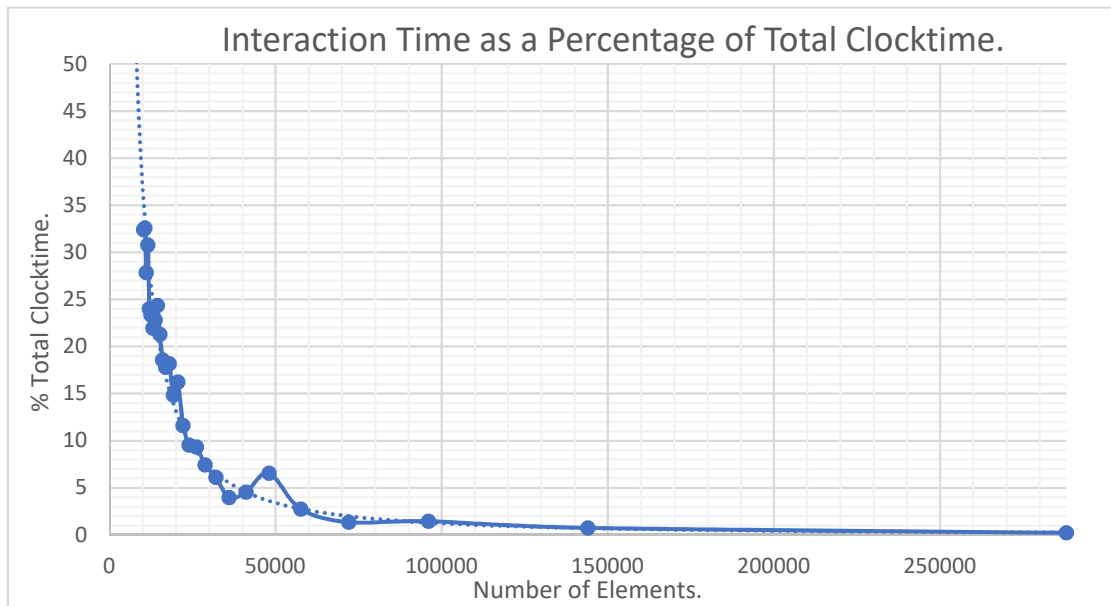


Figure 7- Interaction time as percentage of total clock time against number of elements.

The interaction time as a percentage of the clock time was then graphed against the number of elements, an exponential line of best fit was added. It can be seen that interaction time also reaches 50% at 9000 cells. Past this value, the solution is taking longer to interact between cores than it does computing the solution. From these two graphs therefore, it was decided that 9000 cells per core proved the most efficient when running on the cluster.

4.2. Geometry Creation.

4.2.1. Rectangular



Figure 8 - a) Initial tank geometry. b) Tank with industrialising insert.

The rectangular tank was originally made as a replica of the Armfield W7 Model Sedimentation Tank test bed [40], shown in figure 8a. After preliminary CFD simulations, the design was determined to be too efficient, around 85% of disperse phase was settling and leaving through the underflow. Whilst this may appear successful, it is important to emulate a tank used in industry. In industry, that figure is closer to 50%. This is because the test tank was designed for educational purposes, rather than industrial experimentation. To correct this, an insert was made and placed into the tank, utilising a hopper system and an angled bed reducing sediment build-up (figure 8b). This replicated the effect of a scraper running along the bed collecting settled particles and common in industry, producing results with increased validity. The lower volume decreased cell count by 23% reducing computational time.

4.2.2. Swirl-Flo®

The Swirl-Flo® geometry cross-section shown in figure 9, was made using SOLIDWORKS 2017. An approximate schematic was provided for referencing during its development. In the cases where the schematic was not sufficiently clear, parts were measured manually. The apparatus was provided by Hydro International, and therefore no further modification was necessary. The objective of the build was to finish with the highest fidelity possible, especially around the areas of interest such as the deflector plate and tray. The outer shell, which includes

the tray, overflow, dip plate, inlet, deflector plate and underflow was the main component in the assembly. It was decided that reducing the total number of parts would reduce CAD clean up time. The baffle and internal cylinder/cone setup was then added to complete the design.

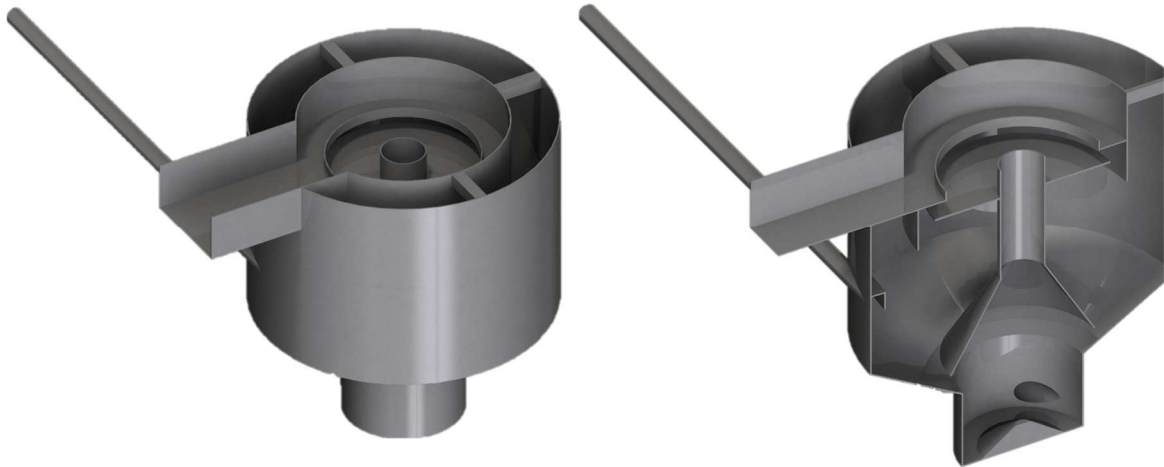


Figure 9 - a) Swirl-Flo Geometry. b) Cross section.

4.3. Structured Mesh Creation - Settling Tank

4.3.1. Convergence Study

A mesh convergence study investigates the relationship between the number of elements in a volume (n) and accuracy of its results. Via an iterative process, results are recorded on a progressively finer mesh. The aim is to gauge the most efficient number of cells giving the most accurate solution. Figure 10 shows the exponential relationship between average nodes spacing (Δs) and the computational time in seconds. Δs is exponentially related to computational cost, therefore, a small difference in node spacing will have a significant effect on computational time. The range of elements tested within this study is 320,000 – 3,100,000 cells, it should be noted that all meshes were structured and refined using the ‘refine.glf’ glyph script [41].

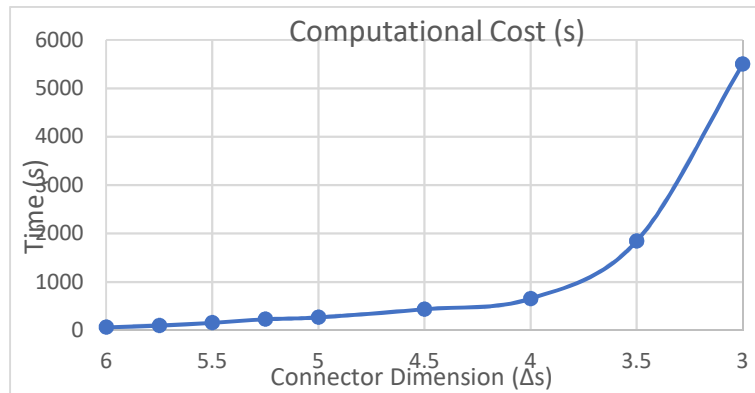


Figure 10 - Exponential relationship between connector dimension (Δs) and computational cost (s).

4.3.1.1. Convergence

Table 1 - Convergence data for settling tank study.

Connector Dimension (Δ_s)	Number of Elements	Computational Cost	Overflow Velocity U (m/s)	Error (ϵ)	Mod Error (ϵ)	%Error
6	320000	62	0.0374767	0.0137911	0.0137911	26.90012054
5.75	408000	98	0.0426854	0.0085824	0.0085824	16.74033214
5.5	466000	154	0.0464614	0.0048064	0.0048064	9.375085336
5.25	527000	228	0.0484367	0.0028311	0.0028311	5.522179614
5	670000	267	0.049974	0.0012938	0.0012938	2.523611312
4.5	881000	436	0.0502658	0.001002	0.001002	1.95444314
4	1281000	654	0.0509235	0.0003443	0.0003443	0.67157163
3.5	2000000	1842	0.0508858	0.000382	0.000382	0.745107065
3	3100000	5502	0.0512678	0	0	0

Table 1 shows data for the study. All the meshes were run using `simpleFoam` to reduce study turnaround, it was estimated that running the study with `driftFluxFoam` would take several months. Before simulation each mesh passed `checkMesh` and run on a single core on equivalent architecture.

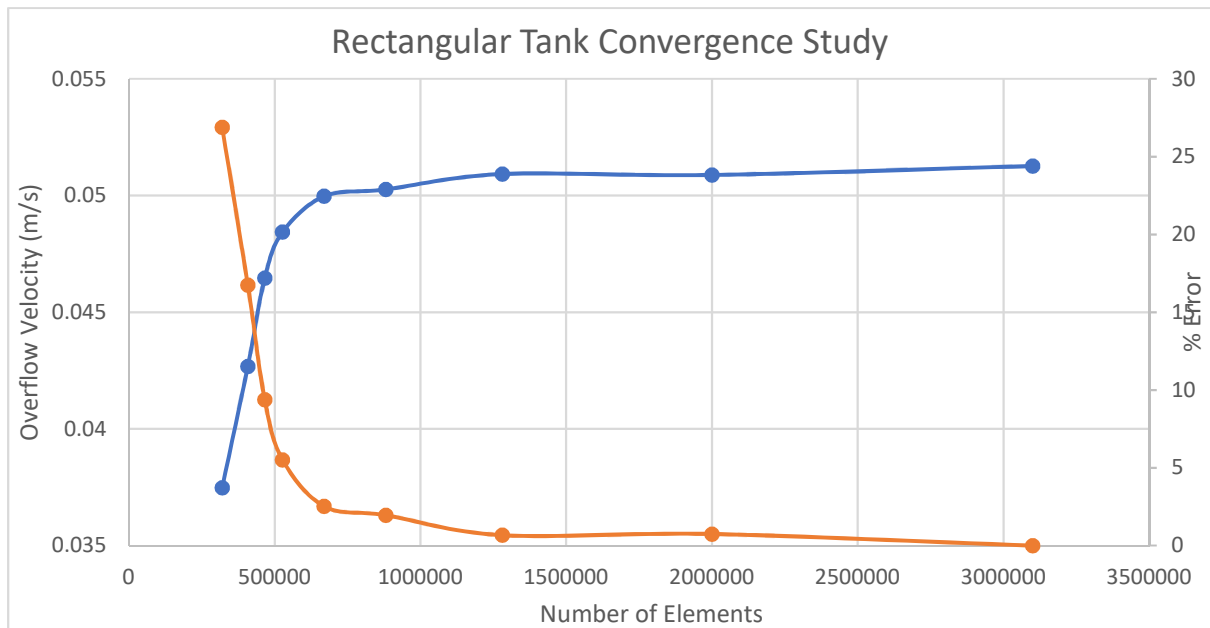


Figure 11 - Overflow Velocity (m/s) and % error against number of elements for the settling tank study.

Figure 11 shows Overflow Velocity (m/s) was found to converge at around 670,000 cells, where the error drops below 2%. It was determined that the 95% reduction in computational time outweighed the discrepancy in the accuracy of the result. The error percentage is calculated against the finest mesh of 3,100,000 cells for this case.

4.3.2. Scaffold

Once the geometry was completed, it was converted to IGES format for compatibility with Pointwise®. Within Pointwise®, the CAD was cleaned up on import using a model assemble tolerance of 0.1, fusing adjacent models and quilts. Then, all outer walls were removed, leaving just the internal volume to be meshed.

Planning and implementing the structured scaffold is arguably the most important factor in efficiently creating a structured grid. Scaffold plans are shown in figure 12. Initially, the imported model was cut along the y-axis plane, 5mm above the outlet weir. This provided a water level height, measured by the experimental team, to significantly reduce `driftFluxFoam` run times.

Inlet Weir - It should be noted that the secondary inlet for slurry was removed. With a diameter of 7mm, the grid would have required unnecessary refinement. Instead, the simulation team agreed that the use of one 30mm inlet with premixed slurry would not impact on simulation results. This allowed for a much simpler scaffold at the inlet weir, which also reduced the cell count. Because structured grids rely on regular connectivity, the high level of refinement on the surface mesh would have been extruded through the volume. The inlet itself was meshed with an OH butterfly topology.

Hopper – The hopper scaffold was based on an OH-topology, this was necessary due to the circular underflow. The figure 13c shows how it adapts to the square perimeter as it expands and rises.

Inlet and Underflow Pipes – Fully developed flow is defined as flow with no velocity gradients in flow direction, it is very important that the flow entering the settling tank is fully developed when validating a simulation. The distance fluid travels in a pipe before becoming fully developed is known as its ‘entrance length’, this is defined as:

$$L_h = 1.395 R_e D^{\frac{1}{4}} \quad (8)$$

For turbulent flow. Where L_h is entrance length, R_e is the Reynolds number, and D is pipe diameter. Using this equation, an entrance length of 412mm was calculated. In his book, “Essentials of Fluid Mechanics”, Cimbala et al [42] deliberate the reduced dependence on R_e in turbulent flows. From a practical engineering perspective, they found entrance effects became insignificant beyond an inlet pipe length of 10 times its diameter. To aid computational efficiency, the inlet pipe length was therefore approximated as

$$L_h = 10D = 300\text{mm} \quad (9)$$

The underflow pipe length was less critical as flow will have already developed in the tank, so the length was halved to

$$L_h = 5D = 150\text{mm} \quad (10)$$

Reducing computational time.

Main Volume – The scaffold for the main volume was divided into 4 tiers along the y-axis for areas of significance: floor, inlet weir height, outlet weir height and free surface. It was important that the hopper topology was carried through the tiers.

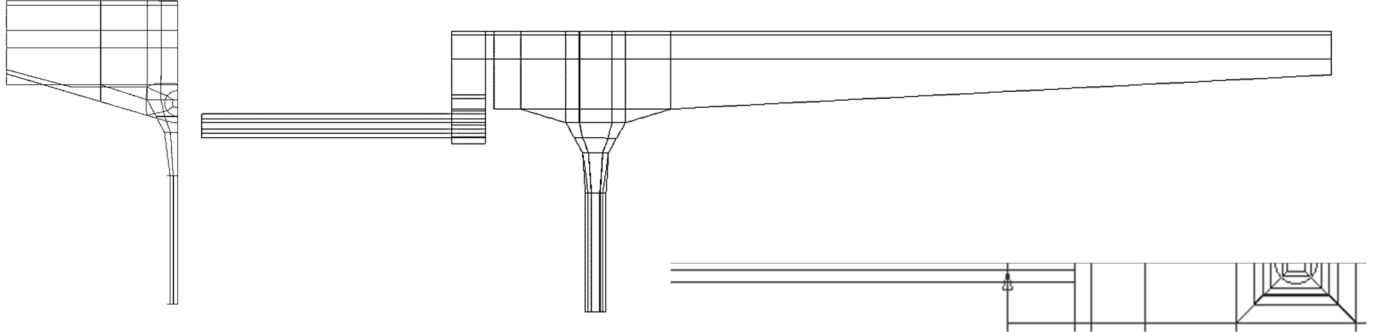


Figure 12 - Rectangular tank structured scaffold a) x-axis plane b) z-axis plane c) y-axis plane.

4.3.3. *Elliptic PDE Solver*

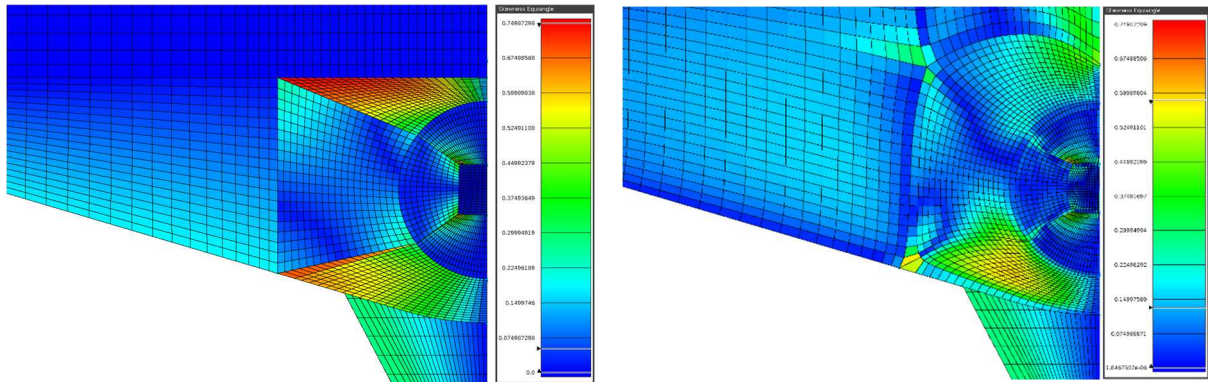


Figure 13 – a) Inlet region a) before elliptic solver application and b) after elliptic solver application.

Once the scaffold was filled with structured blocks, the mesh was examined, and areas of high skew highlighted. The O-type cells surrounding the inlet pipe exhibited the highest skew. Due to the large hopper width in the centre of the mesh, the scaffold forced a wide birth around the circular topology, skewing the hexahedral. Figure 13 shows how the elliptic solver was implemented to smooth out skew and increase orthogonality in the region. To do so, all interior edges were set to orthogonal with a Steger-Sorenson boundary model and the solver run for 5 iterations. This enabled points on connectors to move to a position that more favourably tolerates orthogonality. Then, all exterior edges received a fixed edge function whilst all internal stayed floating. This was run for 50 iterations, dropping skew from 0.7498 to 0.5865, a drop of ≈ 0.16 . This significantly increased the mesh compatibility with OpenFOAM® and driftFluxFoam.

4.3.4. Boundary Layer

The inclusion of boundary layers was effected using the distribution tool. A boundary layer of 1.6mm was calculated for a y^+ value of 35 [43]. This value was chosen because it is found within the $30 < y^+ < 300$ boundary specified for the RealizableKE turbulence model [44]. The wall spacing was calculated using Pointwise®'s y^+ calculator which is based on Frank M.White's book "Viscous Fluid Flow" [45]. Should turbulence be placed within the `driftFluxFoam` simulations it is important that activity at the boundary is correctly modelled.

4.3.5. Export

When exported through the Computer Aided Engineering (CAE) tab, the OpenFOAM® solver was selected and boundary conditions set. All domains received a boundary of 'wall' except for those running along the z-axis symmetry plane which received the 'symmetryPlane' condition. The inlet, underflow, overflow and free surface domains received a 'patch' boundary condition.

4.3.6. Structured Grid – Rectangular Settling Tank



Figure 14 - Final multi-block structured grid.

The final structured Pointwise® mesh used a 94 multi-block structure and took a total of 10 hours to construct. It had maximum centroid and equiangular skew of 0.408 and 0.58 respectively. Interior angles of all quadrilaterals were between $32^\circ > \theta > 148^\circ$. CheckMesh values are shown in table 2. The structured topology ensured a low maximum and average non-orthogonality. It also meant neighbouring cells could be found directly via the structure as opposed to an unstructured mesh where a connectivity table must be maintained and queried

to find neighbouring points. These factors contribute to faster computational times. The hopper design's OH topology is shown in figure (15) alongside its equiangle skewness attributes.

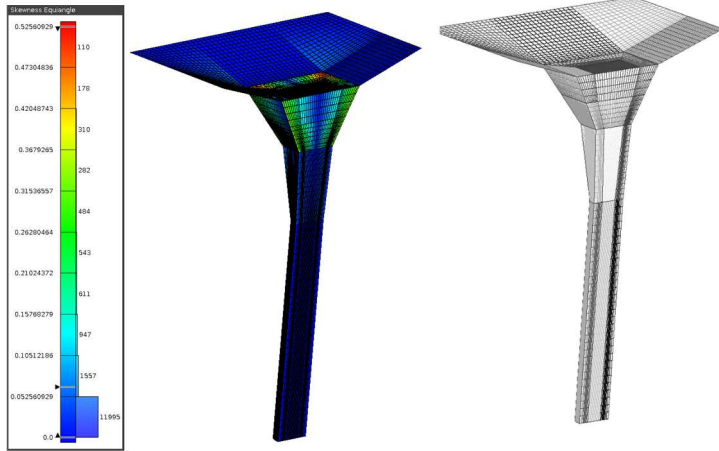


Figure 15 - Hopper OH design. a) Within examine function. b) Observable multi-block function.

The mesh performed well [46], running `driftFluxFoam` quickly and efficiently within the time scope of the report. It also performed when solved using an adjoined solver. This mesh was used as a benchmark when attempting to create a valid computational model for OSP.

Table 2 - `checkMesh` results for structured grid.

Max Aspect Ratio	Max Non-orthogonality°	Average Non-orthogonality°	Max Skewness	Total Cells
20.38	35.4	5.9	1.77	629,466

4.3.7. Pointwise® Automation Study

An attempt was made to automate the process of creating the structured grid shown in 4.3.6. Whilst pointwise is a *bottom up* meshing tool, it can be utilised as a top-down program in some respects. A technique devised by S. Daniels at Exeter University seeks to automatically change the mesh in some respects through the use of journaling. Whilst it would be impossible to perform this technique around a new geometry, it is possible edit an existing topology. In this example a script was created to edit the free surface height above the outlet weir.

4.3.7.1. Methodology

The completed grid shown in 4.3.6 was edited so that the top tier and all its vertical connectors were deleted. This was then saved as ‘automatedWaterHeight.pw’ in an automation study directory, a new Pointwise® file created, journaling turned on and ‘automatedWaterHeight.pw’ reloaded. The top tier of the mesh was then re-built whilst journaling recorded GUI operations. In this instance to re-build the free surface tier, the outlet weir tier was copied and translated upwards by a fixed value before being re-blocked. The translation vector can be found in the journal file:

```
pw::Entity transform [pwu::Transform translation {0 5 0}] [$_TMP(mode_3)]
```

As shown above, the translation vector was 5mm in the positive y direction. The aim of this exercise was to change the translation vector y value ‘5’, to a user defined value set within a source file. To do this, the source file ‘waterHeightLevelUser.glf’ was added to the directory in which the journal file ‘waterHeightLevel.glf’ was kept. It was then read into ‘waterHeightLevel.glf’ by adding the following lines to the beginning of the script.

```
set scriptDir [file dirname [info script]]
source [file join $scriptDir "waterHeightLevelUser.glf"]
```

Next the translation vector code was edited so that it referenced waterLevelHeightUser.glf, by creating a list vector and using \$ to reference it.

```
pw::Entity transform [pwu::Transform translation [list 0 $waterHeightLevel 0]]
[ $_TMP(mode_3) getEntities ]
```

Then, waterHeightLevelUser.glf was edited, by entering an amended value, for example:

```
Set waterHeightLevel 7
```

The free surface height above the outlet weir was then amended to 7mm when running the script through Pointwise®. This method could be used multiple times in one script to automatically make numerous changes.

4.4. *Hybrid Mesh Creation - Swirl-Flo® Tank*

To make a fully structured, multiblock grid of the Swirl-Flo® tank was considered unfeasible within the time scope of the report. Instead, a hybrid topology was formulated with the aim of reducing mesh construction times. The mesh was to include a structured centre cone, inlet and underflow sections. Elsewhere, the tank volume was to be unstructured, initialised with a T-Rex® boundary layer. This enabled flexibility and a quick re-mesh should an optimisation study be required. The quality objective for this mesh was a maximum centroid skew of 0.7, a maximum included angle of 160° and no non-orthogonal cell faces.

4.4.1. *Convergence Study*

A mesh convergence study equivalent in method to section 4.3.1 was also applied to the Swirl-Flo® tank. However, all meshes were unstructured, tetrahedral and with no T-Rex® Boundary Layer. This study provided target values for preparing the final grid to ensure a valid result, without the wasting extensive project time.

4.4.1.1. Convergence data.

Table 3 - Convergence data for Swirl-Flo study.

Connector Dimension (Δ_s)	Number of Elements	Computational Cost (s)	Overflow Velocity U (m/s)	Error (ϵ)	Mod Error ($ l $)	%Error
16	263000	51	0.145382	0.034861	0.034861	19.3411172
14	387000	105	0.14823	0.032013	0.032013	17.76102262
12	558000	206	0.153064	0.027179	0.027179	15.07908768
10	895000	550	0.161629	0.018614	0.018614	10.32716943
8	1552000	1145	0.164811	0.015432	0.015432	8.561774937
7	2521000	2379	0.172193	0.00805	0.00805	4.466192862
6	3265000	4682	0.173692	0.006551	0.006551	3.634537818
5.5	3945000	7428	0.176973	0.00327	0.00327	1.814217473
5.25	5535000	15435	0.17831	0.001933	0.001933	1.072441093
5	6190000	20435	0.17881	0.001433	0.001433	0.79503781
4.5	7570000	26478	0.178815	0.001428	0.001428	0.792263777
4	8894000	43672	0.179592	0.000651	0.000651	0.361179075
3.5	13805000	60597	0.180243	0	0	0

Table 3 above shows data for the study. All the meshes were run using `simpleFoam` to reduce study turnaround, it was estimated that running the study with `driftFluxFoam` would take several months. Before simulation each mesh passed `checkMesh` and was run on a single core on equivalent architecture. The range of cells used within this investigation is 263,000-13,805,000. The exponential relationship between Δ_s and computational cost is equivalent to figure 10 and therefore not repeated.

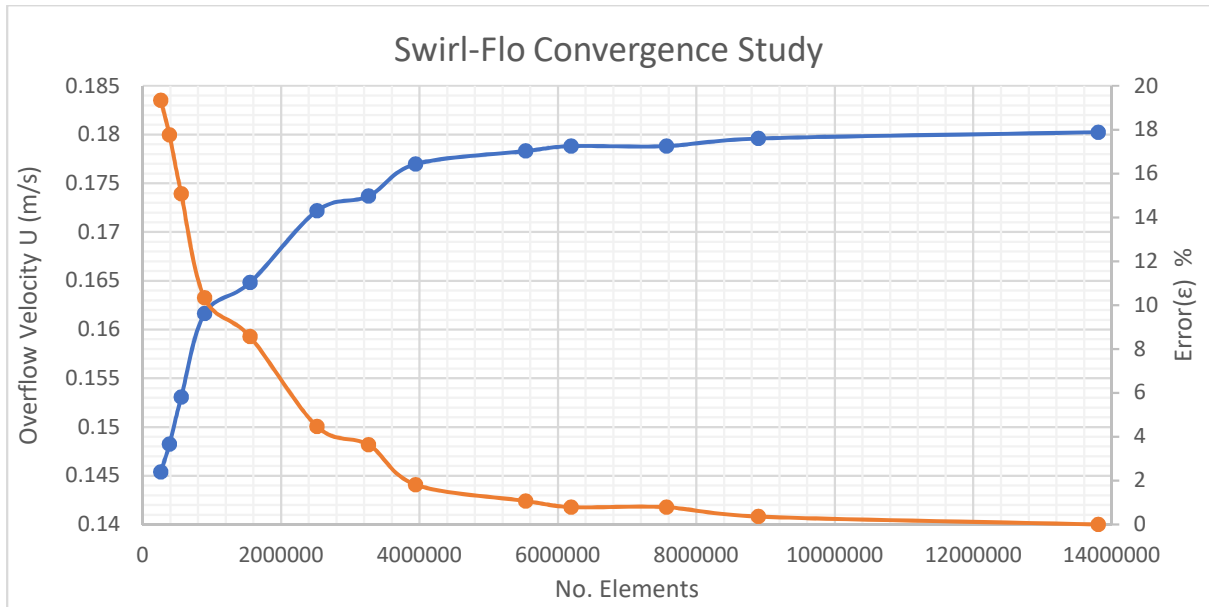


Figure 16 - Overflow velocity (m/s) and % error against No. elements.

Figure 16 shows Overflow Velocity and Error % against No. Elements. The error percentage is calculated against the finest mesh of 13 million cells. The error drops below 1% at ≈ 5.5 million cells. The tolerance was finer for this study compared to its structured counterpart (4.3.1) due to the unstructured nature of the mesh. The aim going forward therefore was to generate a hybrid, unstructured mesh with a T-Rex® extruded boundary layer totalling 5.5-6 million cells.

4.4.2. Hybrid Scaffold

The hybrid scaffold consisted of 3 structured grids, shown within figure 17 in blue, encompassed within an unstructured grid, shown in black. All structured grids were made using an OH butterfly topology, solved using the elliptic solver with Thomas-Middlecoff interior control function, Steger-Sorenson boundary control function and a floating edge function on all interior edges. This resulted in a maximum Centroid Skew of 0.21 and an average of 0.03. The remaining unstructured surface domains were blocked and initialised using T-Rex®.

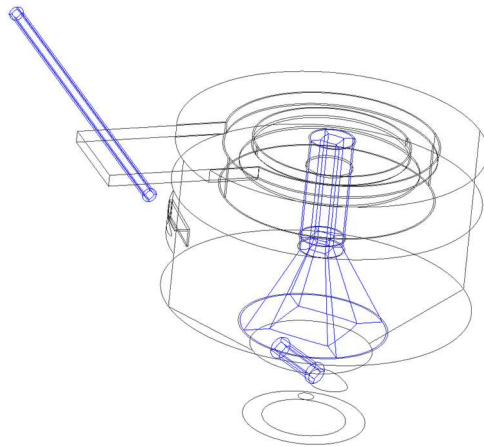


Figure 17 - Swirl-Flo Scaffold.

4.4.3. T-Rex Block Initialisation

4.4.3.1. Surface Mesh

When initialising a block with T-Rex®, it is imperative to start with a high quality surface grid. A surface grid with a maximum equiangular skew of 0.59 and included angles in the range of 20° - 160° was created. Figure 18 shows the area ratios on the surface mesh for the deflector plate region. Particular attention was paid to domains neighbouring an interior connector (highlighted in orange), cells either side should be of approximately equivalent area [28]. It was important to keep area ratio below 1.5 on all cells neighbouring the interior connectors, enabling T-Rex® to smoothly map its surface. Figure 18 shows an average of 1.35 was achieved.

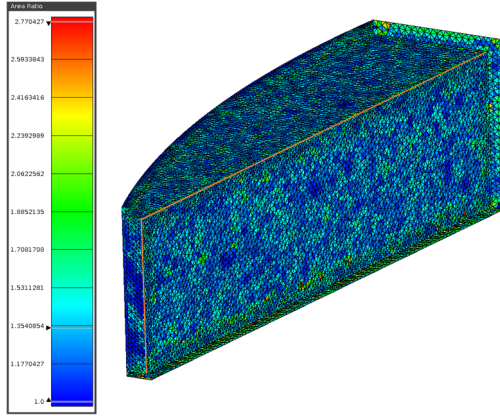


Figure 18 - Area ratios for the Deflector Plater region.

4.4.3.2. Parameters

Once the surface meshed was completed, the domains were blocked and initialised. To do this, the parameters in table 4 were identified as creating the highest quality mesh. For more information regarding the parameters see section 3.1.4.1.

Table 4 - T-Rex Parameters.

Parameter	Value
Max Layers	100
Full Layers	2
Growth Rate	1.1
Isotropic Seed Layers	3
Collision Buffer	5
Max Angle	150
Max Centroid Skewness	0.5

The maximum layers function was set to an arbitrarily large number, this ensured that all layers extruded to isotropy, ensuring a smooth blend to the tetrahedral centre volume. Full layers was set to a non-zero value. This ensured a complete layer across the tank. A geometric growth rate of 1.1 was chosen to match that of the shared structured domains, aiding quality at the structured/unstructured interface. Isotropic seed layers helped to blend any fronts stopped locally by skewness criteria, to blend with the tetrahedral volume. The collision buffer was set to a large value of 5 to accommodate the complex nature of the geometry. When smaller values were specified, the cavity between fronts did not have the capacity for uncompressed tetrahedra (see figure 19). Maximum included angle and centroid skewness parameters were placed low in an attempt to keep the mesh quality high.

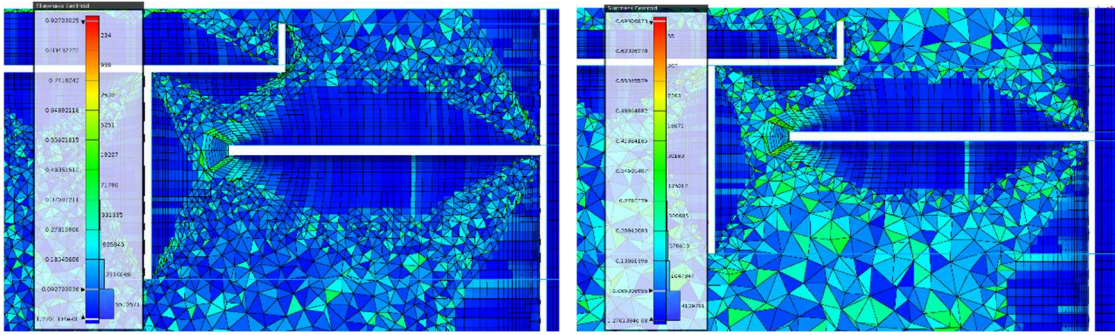


Figure 19 - The complex tray region with a collision buffer of a) 0.5 and b) 5.

4.4.3.3. Initial Spacing

The initial wall spacing (Δs) varied depending on where the wall was positioned within the geometry. A simpleFoam simulation was run on a mesh with no T-Rex[®] extrusion and velocity values at the perimeter of the tank on a y-axis plane collinear with the deflector plate ($y = -0.26\text{m}$) were noted. These are shown in table (5a).

Table 5 - Perimeter coordinates and their respective a) Velocity (m/s) b) Initial wall Spacing (mm) values.

Coordinate	Velocity (m/s)	Coordinate	Initial Wall Spacing (mm)
0.3, -0.26, 0	0.287057	0.3, -0.26, 0	1.946
-0.3, -0.26, 0	0.02342	-0.3, -0.26, 0	19.945
0, -0.26, 0.3	1.23879	0, -0.26, 0.3	0.5
0, -0.26, -0.3	0.135782	0, -0.26, -0.3	3.9

The table (5b) shows the calculated wall spacing for each co-ordinate on the circumference of the Swirl-Flo[®]. Using Pointwise[®]'s wall spacing algorithm [43] the following values were input: the relevant velocity (table 5a), the kinematic viscosity for water at 20°C, a desired y^+ value of 30, and a reference length of 0.6m (diameter of Swirl-Flo[®] tank). An initial spacing of 20mm was deemed too high for the stagnant region of low velocity behind the deflector plate, because the mesh quality was very poor when T-Rex[®] attempted to smooth between 0.5mm and 20mm. A general initial spacing (Δs) of 0.5 would be chosen, to aid mesh quality and allow the T-Rex to grow to a sufficient number of layers to reach isotropy. This ensured that boundaries widths at all speeds were modelled. In specific areas of small volumes, the value was reduced to improve quality.

The subsequent mesh was extruded and enhanced within Pointwise[®] using the 'tweak' tool. The 'tweak' tool enables the user to manually amend volume blocks and surface triangles to lower maximum skew values. To do this, the 'extrema' tab within the 'examine' tool was used to locate the coordinates of the cell with maximum skew, those coordinates were then entered

into the ‘tweak’ tab and the local node moved to relieve the cell. This process was repeated until the maximum centroid skew was below 0.7 [12].

Once this was achieved the subsequent mesh was exported to OpenFOAM® for checkMesh and simpleFoam assessments. Various aspects of the mesh quality are discussed below.

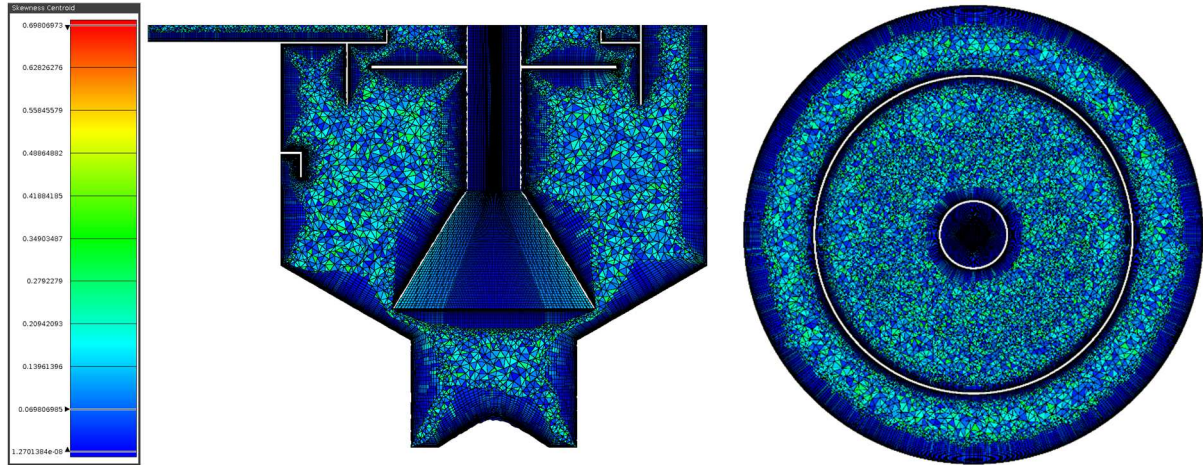


Figure 20 - Cross sections through a) z-axis plane through mesh centre b) y-axis plane through tray region.

Figure 20 shows complete layers with a maximum centroid skew of 0.69, conforming to the initial aim of keep skewness below 0.7. The average skew amounted to ≈ 0.07 confirming a high quality, boundary mesh was completed. Figure 20a also shows the structured topology in the central cylinder of the mesh. All boundaries were grown to isotropy or stopped locally by parameters defined in table 4, and this is evident in the non-consistent local maximum T-Rex® layer heights across the surface.

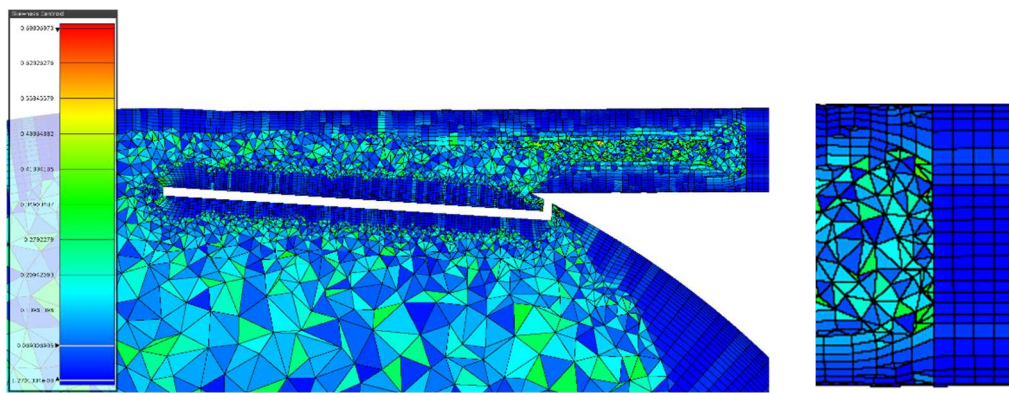


Figure 21 - a) Deflector plate region b) Close up structured/unstructured boundary layer interface.

It’s possible to see a high quality boundary layer cross section along the y-axis plane for the deflector plate region in figure 21a. An area of high interest, the section was comfortably meshed with a tetrahedral prism layer. The ‘distribute’ tool was used on the structured

connectors to ensure volume ratio stayed consistant between structured and T-Rex® boundary layers, this technique was used for the underflow with equivalent results. The total cell count for the mesh was 6,271,337, above the target of 5.5million set in section 4.4.1.

Pointwise® does not have an orthogonality check integrated within the software. To check this, each mesh was exported via CAE and written into a case file, where the `checkMesh` function was performed in OpenFOAM®. A recurring issue with non-orthogonality was observed, mainly around the baffle plate and tray region, where multiple non-orthogonal faces were created. Unfortunately, a maximum non-orthogonality of 81.3863° was found with a total of 354 of 15,245,650 non-orthogonal faces. Due to the volatility of OpenFOAM® solvers, especially the predictive-corrective nature of `driftFluxFoam`, non-orthogonal faces are not tolerated. This can be attributed to the way in which OpenFOAM® solves through face normal. Two non-orthogonal faces adjacent to each other would cause divergence between cells (section 3.1.3.2).

4.4.4. Improved Hybrid Scaffold.

In an attempt to avoid this, a new Hybrid scaffold was designed to mitigate against non-orthogonal faces. Within this new scaffold, the whole tray area was structured, with the T-Rex® boundary layer occurring along an x-axis plane at the bottom of the dip plate. This way, the tray area received a high quality, structured mesh with a distribution tool influenced boundary layer, mitigating against non-orthogonal faces. The main body of the tank remained an unstructured T-Rex® volume, taking advantage of its flexible attributes, allowing for optimisation.

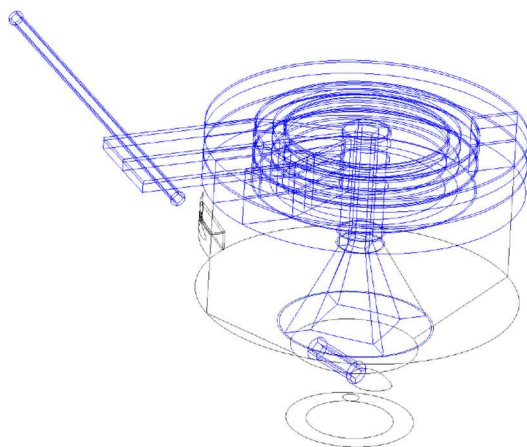


Figure 22 - Improved Scaffold with Structured Tray.

The tray region comprises mostly of O-type hexahedral cells, due to the Swirl-Flo®'s cylindrical shape. A multiblock structure was devised and implemented by creating a y- axis

plane based template for each geometrical feature of the tray and dip plate region, and then extruded up the y-axis from the bottom of the dip plate. Figure 23 and 24 show various aspects of the completed hybrid topology. Special attention was paid to the overflow tray region, here the cells convert to H-type hexahedra to accommodate the rectangular shape of the overflow shown in figure 23b.

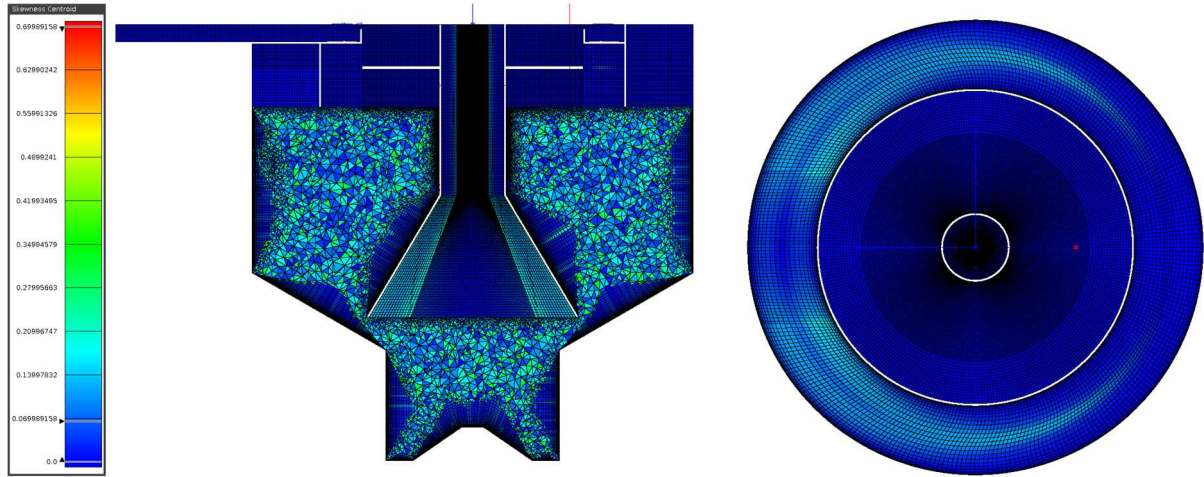


Figure 23 - Cross sections of improved mesh a) z-axis plane through mesh centre b) y-axis plane through structured tray region.

The T-Rex® formations below the tray can be seen for the central and underflow regions of the tank in figure 24. The T-Rex® parameters for these were unchanged.

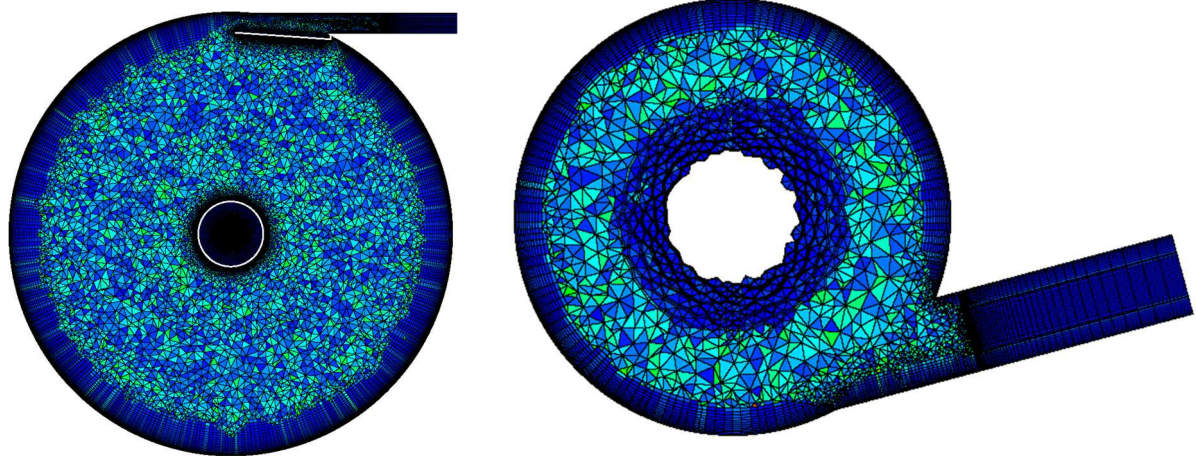


Figure 24 -Cross Sections of improved mesh a) y-axis plane collinear with inlet. b) y-axis plane collinear with underflow.

4.4.5. **checkMesh Failure.**

Table 6 – CheckMesh results for both Swirl-Flo® meshes.

Mesh Topology	Max Aspect Ratio	Max Non-orthogonality°	Average Non-orthogonality°	Non-Orthogonal Faces	Max Skewness	Total Cells
Unstructured Tray	27.6978	81.3863	17.53	354	2.40	6,271,337
Sturctured tray	25.2933	75.6	13.6512	43	2.1994	4,686,638

Table 6 shows checkMesh results for both meshes. A reduction in maximum values of aspect ratio and checkMesh skewness was observed in the new mesh. Regrettably, with a reduced maximum non-orthogonality of 75.6° , 43 non-orthogonal faces persisted. This large reduction in non-orthogonality still resulted in divergence when solving through the mesh using driftFluxFoam. Removed from the tray/baffle region, some were present at the structured/unstructured interface, deflector plate and a few suspended in tetrahedral volume. Figure 25 shows the non-orthogonal faces represented in red for both meshes.

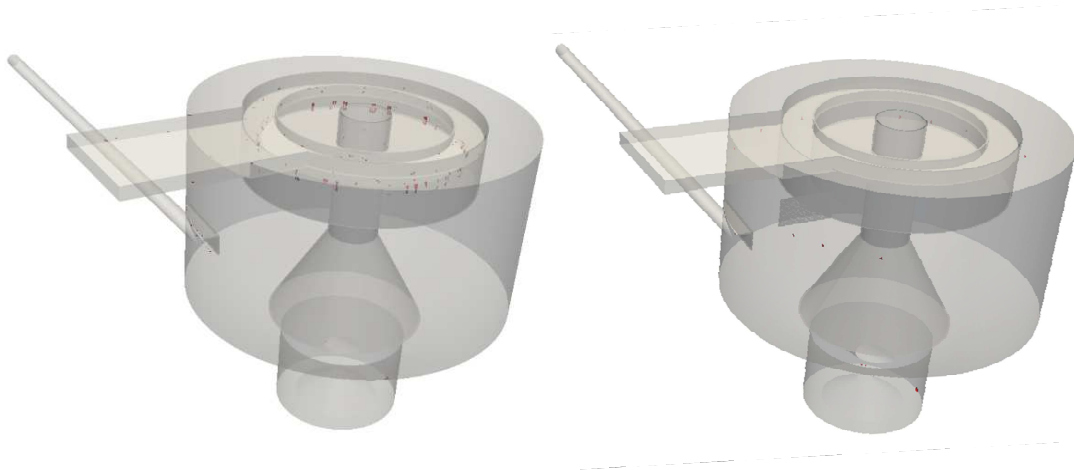


Figure 25 - Non-Orthogonal faces in a) original Swirl-Flo mesh. b) improved structured mesh.

5. Discussion and conclusions

5.1. Discussion

The strengths, weaknesses and capabilities of Pointwise® are discussed in this report. The majority of Pointwise® features were used to create computational grids on both a sedimentation tank and hydrodynamic vortex separator. All decisions taken during scaffold and grid topology creation are explained. As anticipated, the structured meshing framework in Pointwise® offered facilities to create high quality structured grids for the rectangular sedimentation tank. It proved robust enough to run even the most complex solvers, including adjoint solvers. The distribution tool allowed for the creation of a quality boundary layer on the simple geometry of the rectangular tank. Whilst the results of the simulations did not show good agreement with empirical data, this was not attributed to mesh quality. Pointwise®'s glyph feature was used extensively when creating the mesh. In order to increase user efficiency, open source macro scripts “Create OH” [29] and “Refine” [47] were used during construction. A template script for small automated design changes was also attempted. The

subsequent script was used to create multiple meshes with different free surface heights quickly and efficiently, for experimentation by other members of the group. Whilst this was a simple case, the methodology could be expanded for other optimisation techniques, however it was observed that this method would not be sufficient to model added parts within the geometry.

The majority of this report is focussed on the use of T-Rex[®] as a tool for unstructured and hybrid meshing techniques. These techniques are central to current industry methods, especially at structured/unstructured interface regions in hybrid meshes. The meshes created in this report are of high quality, and have potential to accurately model single-phase flow. This was shown by good performances when used to run the `simpleFoam` solver. Results in the unstructured and structured tray hybrid swirl-Flo meshes were within 3% of the completely unstructured, high fidelity 13,000,000 cell mesh used as a bench mark for performance, despite having 54% and 71% less cells respectively. However, T-Rex[®] could not perform effectively when solving multi-phase flow, specifically `porousDiftFluxFoam`. Its function is to create anisotropic, right-angle tetrahedra off a boundary, creating high levels of face skew for cells near and adjacent to the cylindrical wall, due to small initial spacing parameters. For example, the initial spacing in the deflector plate region was smaller than on the main walls of the tank, increasing the risk of skewed cells off the surface of the mesh. It was noted that 28 of 44 non-orthogonal faces are present within this region for the final hybrid mesh in this report. Other factors such as restricted volume for advancing fronts may also exacerbate non-orthogonality.

Multiple techniques were employed to try to mitigate the non-orthogonal effects, such as extreme surface refinement on the deflector plate. This refinement reduced aspect ratios of the anisotropic cells relative to their initial spacing. Fronts also reached isotropy more quickly, creating space for the formation of unstructured tetrahedra. Still, non-orthogonal faces persisted in tiny quantities relative to the total number of faces. Two methods not used in this report would have guaranteed the removal of non-orthogonal faces. The first is to remove boundary layers completely and simply use an unstructured hybrid mesh. Whilst this is a possibility, it would eliminate the ability to accurately model turbulence within the separator. The performance of a hydrodynamic separator is measured by its efficiency in the removal of suspended solids. It does so by reducing its velocity heavily at the walls, forcing its removal from the vortex. Incorrectly modelling the viscous effects of the boundary layer would have a profound effect on this [48]. The second is to mesh the tank using a completely structured approach. This would allow for high quality results with a boundary layer and good quality

metrics throughout. This approach wasn't attempted in this study for two reasons. Firstly, by creating a completely structured mesh, the flexibility for automation during an optimisation study is dramatically reduced and optimisation studies would take far longer to complete. Whilst there are automation tools in industry for structured meshes, the complexity of the geometry would be prohibitive. Secondly, this investigation sought to review multiple meshing techniques. As the industry focus turns to unstructured grids, it is imperative these are improved through further research.

5.2. Future Work

T-Rex is a powerful tool, despite demonstrable room for improvement. Further investigation into its use is important for internal meshing. Encroaching fronts compressing tetrahedra and structured/unstructured interface regions within confined volumes are of particular interest for future study. Should this project be continued, considerable research into using T-Rex[®] for OpenFOAM[®] would be completed. It appears that the different approaches between Pointwise[®] (stores points and cells) and OpenFOAM[®] (stores faces and cells) has meant that T-Rex[®] is not well optimised for creating internal meshes, which subsequently create non-orthogonality not tolerated by OpenFOAM[®] solvers. This deficiency would be mitigated by analysing mesh performance when used with its more robust commercial rivals, for instance Ansys FLUENT[®]. OpenFOAM[®] would then be used to create equivalent results by using different T-Rex[®] methods such as unstructured multi-block strategy. Peer reviewed literature provides multiple examples of the use of T-Rex[®] to mesh externally into a domain, eliminating the problem of encroaching fronts and finite complex volumes.

A highly refined mesh was created, shown in figure 26, to explore the performance of T-Rex[®] without the constraint of computational capacity. The quality metrics of this mesh are far superior to the grids presented in this paper, with no non-orthogonal faces. This is due to the greatly increased relative space created when T-Rex[®] is meshing with smaller surface edge lengths. However, the total cell count amounted to \approx 60million and solving through this mesh using `driftFluxFoam` on current infrastructure could take upwards of a year. However, with access to a more computer power, it would provide key insight into new T-Rex[®] techniques that could be translated onto coarser meshes.

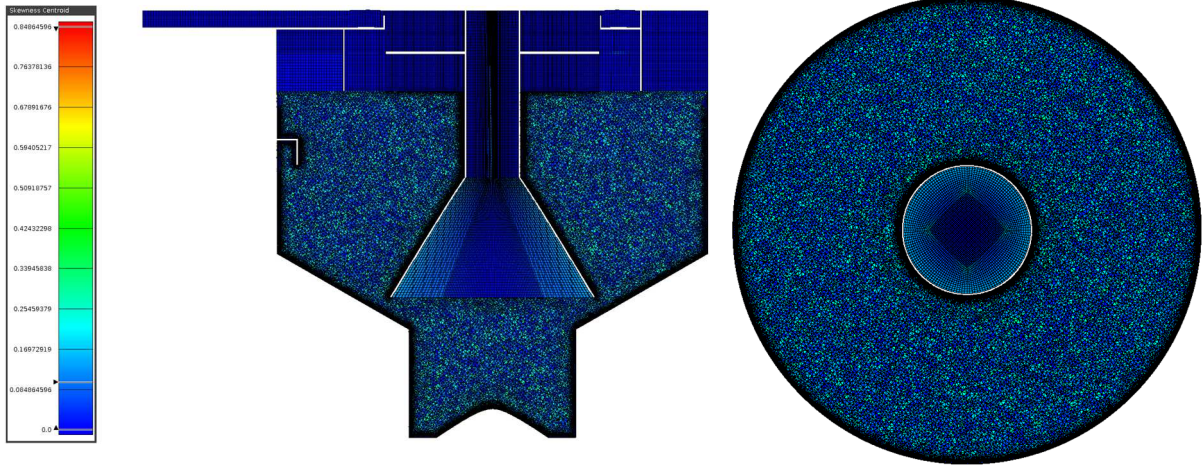


Figure 26 - Cross section of refined T-Rex volume mesh a) z-axis plane through mesh centre. b) y-axis plane below structured tray area.

5.3. Conclusion

In conclusion, Pointwise[®] is very powerful software, used within industry and academia alike, and is a proven tool for CFD pre-processing and mesh generation. Its strengths lie in its compatibility with most CAD software, which allows for easy import of database files; and its unautomated structured and unstructured meshing capabilities, which provide high quality grids. This indicates that the *bottom-up* approach to mesh generation is superior when quality is priority.

Since 2012, Pointwise[®] has sought to influence the automated *top-down* market. Recent versions have seen the release of its own tcl based Glyph journaling toolset and the highly automated T-Rex[®] function. This report identifies shortfalls in the incorporation of automation into the software, indicating opportunities for further development. Even Pointwise[®] professionals have highlighted non-orthogonality issues when using T-Rex[®] meshes such as the DrivAer case [12]. However, should these be addressed in later releases, a fusion of Pointwise[®]'s unparalleled ability to create high quality grids with incorporated quick, easy automation methods, would prove extremely powerful in a CFD industry that revolves around iterative design optimisation.

6. Project management

This report represents one of seven individual reports contributing to “*Experimental and Numerical Investigation into the Use of Olive Stone Powder as a Substitute for Primary Sludge Modelling*” [1]. Prior to the project commencing, the group was split into two teams:

experimental and computational. The computational team was further split into sub-groups: meshing and simulation. It was evident that each team was chronologically dependant on the output of the other. Therefore, a Gantt chart was created to ensure tasks could be completed within individual timeframes, and to track progress. Because of reliance on other members in the group, stratagems were put in to place to mitigate against incomplete or late delivery of work packages. For instance, whilst investigating the use of different programs to avoid duplication, two team members creating meshes provided security to the simulation team. Progress was also tracked during weekly meetings with supervisors. All meetings had a chair and secretary to ensure structured discussion of all relevant topics. To improve communication between the computational team, the team agreed to work in the same location. This project was split into two categories, research for group progression covered in depth in section 7, and individual investigation. Group progression work was prioritised and forward loaded to ensure that group research was completed prior to individual investigations.

Since this is a computation based project, health risks were minimal, but all team members received a laboratory induction prior to project commencement. However, risks to file security and loss were significant. This was mitigated by the use of a SharePoint within Hydro International's intranet. This site provided version control, backup facilities, and sufficient storage to securely store research and relevant material. In addition and in line with CFD custom and practise, a 2TB hard-drive within the work space and used to back up all files and directories too large to efficiently utilise cloud storage.

Over the course of the project, three factors impacted the group project schedule. These had to be managed to ensure deliverables were still met:

Client Scope— As mentioned in section 3.2.2.1, the initial plans for the rectangular tank were to use its simple geometry to enable the author to research mesh generation techniques within Pointwise®. The group intended to utilise its simplicity to create a correct computational model that could be applied to the Swirl-Flo® tank for further analysis. The client subsequently requested that the tank model should be amended to reflect the more complex primary tanks used alongside the Swirl-Flo® separator in industry. This increase in complexity impacted the time required for sedimentation tank settling analysis, impinging on time originally planned for the Swirl-Flo®. It also affected the quality of the empirical data, making computational validation problematic.

Computational Time – The extremely long elapsed computational time required to

complete porousDriftFluxFoam was not considered prior to the project and this impacted the research time available to the CFD team. The resolution was to use a far coarser mesh in the Swirl-Flo® simulations than was originally planned in order to produce date within the project timescale. This had an adverse effect on the accuracy of the results. For the individual report, the project used simpleFoam, a much quicker, single-phase solver, to run convergence studies. As the group objective computational model validation was not achieved, individual project results were based solely on simpleFoam results and quality metrics of the mesh.

Server Downtime – Unscheduled IT infrastructure downtimes totalling approximately 11 days meant that simulations were interrupted throughout the project, often occurring outside working hours. Over the final week of the report, the servers were down for 62 hours. This impacted report writing as Pointwise® and OpenFOAM® were unavailable for analysis during these periods. Mitigation was provided in the form of a 5-day extension to the project deadline. The delays could have been anticipated through the use a project risk log as a pattern of Friday night downtime was observed throughout the project. Should further research be completed on this infrastructure, the IT department would be approached to identify and fix the cause of the recurring downtime. In addition a project risk log would be maintained to identify and mitigate any other threats to the project, before they become issues.

7. Contribution to group functioning

Work presented in this report provides full CFD pre-processing for members of the simulation team, from geometry creation to a finished mesh exported into case files with applied boundary conditions [46] [49]. To ensure the team could start work on computational modelling, it was important to provide early access to exported meshes within case files. The geometries created were used by all project team members. Experimental teams used the geometries during jig design [50] for measuring apparatus and Swirl-Flo® setup, and within the simulation team, they were used for automatic mesh creation within snappyHexMesh® [51]. The structured mesh of the rectangular sedimentation tank was used by the simulation team for critical analysis and computational modelling [46]. Away from this report, the author managed the finances for the group, providing oversight for the budget.

8. References

-
- [1] Baker. A, Bentley. R, Lowe. J, Mendoza. M, Russell. T, Scobell. T, Aaron. W "Experimental and Numerical Investigation into the Use of Olive Stone Powder as a Substitute for Primary Sludge Modelling" Exeter, 2018.
 - [2] Ibisworld.co.uk. (2018). Sewerage (UK) - Industry Research Reports IBISWorld. [online] Available at: <https://www.ibisworld.co.uk/industry-trends/market-research-reports/water-supply-sewerage-waste-management-remediation-activities/sewerage.html> [Accessed 8 May 2018].

- [3] U.S. Environmental Protection Agency (2018). *Preliminary Treatment*. [online] Available at: <http://web.deu.edu.tr/atiksu/ana52/yeni001.html> [Accessed 8 May 2018].
- [4] Saul A. and Ellin D. 1992, Sediment deposition storage tanks. Water Science and Technology, Vol. 25, No. 8, pp. 189–198.
- [5] Gentry, R. Martin, R. and Daly, B. (1966). An Eulerian differencing method for unsteady compressible flow problems. Journal of Computational Physics, 1(1), pp.87-118.
- [6] Reichenbach H. (1965) Ernst-Mach Institute, Frieburg, Germany; private communication.
- [7] Smith, R. (2008). Origins of the Commercial CFD Industry | Symscape. [online] Symscape.com. Available at: <https://www.symscape.com/blog/origins-of-the-commercial-cfd-industry> [Accessed 8 May 2018].
- [8] Chawner, J. (2015). Quality and Control - Two Reasons Why Structured Grids Aren't Going Away | The Connector. [online] Pointwise.com. Available at: <http://www.Pointwise.com/theconnector/2013-March/Quality-Control-Two-Reasons-Structured-Grids-Aren't-Going-Away.html> [Accessed 16 Apr. 2018].
- [9] Koomullil, R., Soni, B. and Singh, R. (2008). A comprehensive generalized mesh system for CFD applications. Mathematics and Computers in Simulation, 78(5-6), pp.605-617.
- [10] Mavriplis, D. (1995). Unstructured Mesh Generation and Adaptivity. [online] Ntrs.nasa.gov. Available at: <https://ntrs.nasa.gov/archive/nasa/casi.ntrs.nasa.gov/19950020607.pdf> [Accessed 16 Apr. 2018].
- [11] Slack, M., Prasad, R., Bakker, A. and Boysan, F. (2000). Advances in Cyclone Modelling Using Unstructured Grids. Chemical Engineering Research and Design, 78(8), pp.1098-1104.
- [12] Carrigan, T. and Landar, M. (2015). Automotive Design Optimization using Pointwise, Sculptor, and OpenFOAM®. [webinar]
- [13] Tabor, G. and Dodwell, T. (2013). *ECM3152: Computational Engineering*. [online] vle.exeter.ac.uk. Available at: http://vle.exeter.ac.uk/pluginfile.php/46398/mod_label/intro/lecture1-slides.pdf [Accessed 17 Apr. 2018].
- [14] Benson, R. (2018). Simulation of Unsteady Propeller Blade Loads Using OpenFOAM® | The Connector. [webinar] Pointwise.com. Available at: <http://www.pointwise.com/theconnector/2014-May/Simulation-Unsteady-Propeller-Blade-Loads-Using-OpenFOAM.html> [Accessed 16 Apr. 2018].
- [15] Carrigan, T., Bagheri, F. and Edge, B. (2018). The Influence of Meshing Strategies on Simulation Efficiency. [webinar] Pointwise.com. Available at: <http://www.pointwise.com/webinars/dvjzcj7e/index.html?submissionGuid=aea81c85-5dc8-4b30-9093-163d26ffdd28> [Accessed 17 Apr. 2018].
- [16] Khawaja, A. and Kallinderis, Y. (2000). Hybrid grid generation for turbomachinery and aerospace applications. *International Journal for Numerical Methods in Engineering*, 49(1-2), pp.145-166.
- [17] Sideroff, C., Carrigan, T. and Matus, R. (2011). Mastering Hybrid Meshing for Horizontal Axis Wind Turbines. [online] Pointwise.com. Available at: <http://www.pointwise.com/webinars/2011-07/Pointwise-Hybrid-Meshing-Webinar-Slides.pdf> [Accessed 20 Apr. 2018].
- [18] Bui, T. (2010). Explicit and Implicit Methods In Solving Differential Equations. Ph.D. University of Connecticut.
- [19] Courant, R., Friedrichs, K. and Lewy, H. (1928). ber die partiellen Differenzengleichungen der mathematischen Physik. *Mathematische Annalen*, 100(1), pp.32-74.
- [20] Pointwise.com. (n.d.). Pointwise Equiangle Skewness - User Manual. [online] Available at: <http://www.pointwise.com/doc/user-manual/examine/functions/equiangle-skewness.html> [Accessed 19 Apr. 2018].
- [21] Zhang, Y., Dompierre, J., Guibault, F. and Vu, T. (2018). Robust and Automatic CAD-based Structured Mesh Generation for Hydraulic Turbine Component Optimization. 23rd IAHR Symposium, 1(10).
- [22] OpenFOAM. (2018). primitiveMeshCheck.C. [online] Available at: <http://github.com/OpenFOAM/primitivemeshcheck.C> [Accessed 23 Apr. 2018].
- [23] M. Goelke, "Element Quality and Checks," Altair University, 2014. [Online]. Available: <https://altairuniversity.com/modeling/element-quality>
- [24] Aguilar, J. and Goodman, J. (2006). Anisotropic mesh refinement for finite element methods based on error reduction. *Journal of Computational and Applied Mathematics*, 193(2), pp.497-515.
- [25] Chawner, J. (2012). Accuracy, Convergence and Mesh Quality. [online] Another Fine Mesh. Available at: <https://blog.pointwise.com/2012/07/05/accuracy-convergence-and-mesh-quality/> [Accessed 8 May 2018].
- [26] Bakker, A. (2006). Applied Computational Fluid Dynamics. [online] Bakker.org. Available at: <http://www.bakker.org/dartmouth06/engs150/07-mesh.pdf> [Accessed 25 Apr. 2018].
- [27] Pointwise.com. (2018). Leaders in CFD Mesh Generation - Pointwise. [online] Available at: <http://pointwise.com/about/> [Accessed 25 Apr. 2018].
- [28] Woeber, C. (2018). Workshop | Using T-Rex to Generate Unstructured Hexahedra for an Automotive Intake. [online] Pointwise.com. Available at: <http://www.pointwise.com/workshops/2015-11-Germany/Using-TRex-Generate-Unstructured-Hexahedra-Automotive-Intake.html> [Accessed 24 Apr. 2018].
- [29] Hoards, J. (2014). CreateOH. GitHub - Pointwise. [GlyphScript] Available at: <https://github.com/pointwise/CreateOH>. [Accessed 24 Apr. 2018].
- [30] Tufts, M. and Kimmel, R. (2018). Stability Equation Based Transition Prediction. Aerospace Sciences Meeting, AIAA SciTech Forum, 3(6).
- [31] Trottenberg, U., Oosterlee, C., Schüller, A., Brandt, A., Oswald, P. and Stüben K. (n.d.). Multigrid. Academic Press.
- [32] Pointwise.com. (n.d.). Pointwise Elliptic Solver – Interior Control Functions - User Manual. [online] Available at: <http://www.pointwise.com/doc/user-manual/grid/solve/structured-domains-and-blocks/attributes-tab/interior-control-functions.html> [Accessed 19 Apr. 2018].
- [33] Thomas, P. and Middlecoff, J. (1980). Direct Control of the Grid Point Distribution in Meshes Generated by Elliptic Equations. *AIAA Journal*, 18(6), pp.652-656.
- [34] Hillenstock, A. (1988). A fast method for the elliptic generation of three-dimensional grids with full boundary control. Numerical grid generation in computational fluid mechanics 88: Proceedings of the Second International Conference, pp.137-146.
- [35] Lavante, E. (1982). Elliptic generation of two-dimensional grids for internal flow calculations. College Station, Tex: Texas Engineering Experiment Station, Texas A&M Univ
- [36] White, J. (2018). Elliptic grid generation with orthogonality and spacing control on an arbitrary number of boundaries. AIM 21st Fluid Dynamics, Plasma Dynamics and Lasers Conference.
- [37] Steger, J. and Sorenson, R. (1979). Automatic mesh-point clustering near a boundary in grid generation with elliptic partial differential equations. *Journal of Computational Physics*, 33(3), pp.405-410.
- [38] Pointwise.com. (n.d.). Pointwise Elliptic Solver – Edge Boundary Conditions- User Manual. [online] Available at: <http://www.pointwise.com/doc/user-manual/grid/solve/structured-domains-and-blocks/edge-attributes-tab/boundary-conditions.html> [Accessed 19 Apr. 2018].
- [39] Rodgers, D. (1985). Improvements in multiprocessor system design. ACM SIGARCH Computer Architecture News, 13(3), pp.225-231.
- [40] Discoverarmfield.com. (2016). W7MKII : Model Sedimentation Tank. [online] Available at: http://discoverarmfield.com/en/products/view/w7mkii/_model-sedimentation-tank [Accessed 26 Apr. 2018].
- [41] Hoards, J. (2014). CreateOH. GitHub - Pointwise. [GlyphScript] Available at: <https://github.com/pointwise/CreateOH>. [Accessed 24 Apr. 2018].
- [42] Cimbala, J. and Cengal, Y. (2004). *Essentials of Fluid Mechanics: Fundamentals and Applications*. 1st ed. Utah: Jenson Books, p.327.
- [43] Pointwise.com. (n.d.). Y+ Calculator - Compute Wall Spacing for CFD. [online] Available at: <http://www.pointwise.com/yplus/> [Accessed 25 Apr. 2018].
- [44] ANSYS "Introduction to ANSYS Fluent - Turbulence Modeling", 2013. [Online]. Available: <https://www.ansys.com/en-GB/Services/training-center/fluids/ansys-fluent-turbulence-modeling>. [Accessed: 28 Apr. 2018].
- [45] White, F. (2011). Viscous fluid flow. 5th ed. New York, NY: McGraw-Hill Higher Education, p.467
- [46] Bentley, R. (2018) *An Investigation into MULES and its Application into Simulating Settling Behaviour in an Armfield Rectangular Settling Tank*. Experimental and Numerical Investigation into the Use of Olive Stone Powder as a Substitute for Primary Sludge Modelling.
- [47] Hoards, J. (2014). Refine. GitHub - Pointwise. [GlyphScript] Available at: <https://github.com/pointwise/refine>. [Accessed 24 Apr. 2018].
- [48] Stendal, E. (2013). Multiphase Flows in Cyclone Separators - Modeling the classification and drying of solid particles using CFD. Ph.D. CHALMERS UNIVERSITY OF TECHNOLOG
- [49] Russell, T. (2018) *The Use of the Drift Flux Model to Simulate a Hydrodynamic Vortex Separator in OpenFOAM*. Experimental and Numerical Investigation into the Use of Olive Stone Powder as a Substitute for Primary Sludge Modelling.
- [50] Wye, A. (2018) *Investigation and Development of a Mathematical Model to Describe the Settling Characteristics of Olive Stone Powder*. Experimental and Numerical Investigation into the Use of Olive Stone Powder as a Substitute for Primary Sludge Modelling.
- [51] Lowe, J. (2018) *Generation of computational grids for model primary sedimentation devices using snappyHexMesh including volume of fluid free surface simulations*. Experimental and Numerical Investigation into the Use of Olive Stone Powder as a Substitute for Primary Sludge Modelling.

